TRANSIENT TEMPERATURES AND INELASTIC THERMAL STRESSES IN GAS-COOLED PERFORATED CERAMIC CYLINDERS WITH INTERNAL HEAT GENERATION

by

STANLEY ROLLIN FIELDS

A THESIS

submitted to

OREGON STATE UNIVERSITY

in partial fulfillment of
the requirements for the
degree of

CHEMICAL ENGINEER

June 1962

APPROVED:

Redacted for privacy

Professor and Head of Department of Chemical Engineering

In Charge of Major

Redacted for privacy

Chairman of School Graduate Committee

Redacted for privacy

Dean of Graduate School

Date thesis is presented April 20, 1962

Typed by Helen Lundgren

TABLE OF CONTENTS

	Page
INTRODUCTION	1
THEORY AND METHODS	2
1. Heat Transfer	2
a. Unit Cells	2
b. Parent Cylinder	6
2. Thermal Stress	8
a. Viscoelastic Theory	8
b. Thermal Stresses in Perforated Geometries	10
c. Boundary Conditions for Thermal Stresses in a Unit Cell	12
d. Transient Unit Cell Temperature Representation in the Thermal Stress Equation	13
3. Method of Analysis	14
RESULTS	18
CONCLUSIONS AND RECOMMENDATIONS	21
TABLE	
I Transient Temperatures in Slabs of Various Thicknesses Without Heat Generation - A Comparison of Mathematical and Approximate Methods of Calculation	29
FIGURES	
1 Perforated Cooled Cylinder	24
2 A Perforated Gas-Cooled Aluminum Oxide Cylinder with Some Conditions for Analysis	25
3 Thermal Conductivity and Other Property Values for Alumina	26
4 Stability of the Finite Difference Approximation of the Unit Cell Heat Transfer Equation	27

FIGURES

		Page
5	Temperatures Used in the Evaluation of the Stability of the Finite Difference Approximation of the Unit Cell Heat Transfer Equation	28
6	Transient Temperature Analysis of a Small Slab - A Comparison of Mathematical and Approximate Methods of Analysis	30
7	Transient Temperature Analysis of a Small Slab - A Comparison of Mathematical and Approximate Methods of Analysis - Total Slab Thickness = 0.6 Inch	31
8	Transient Temperature Analysis of a Small Slab - A Comparison of Mathematical and Approximate Methods of Analysis - Total Slab Thickness = 0.3 Inch	32
9	Transient Temperature Analysis of a Small Slab - A Comparison of Mathematical and Approximate Methods of Analysis - Total Slab Thickness = 0.1 Inch	33
10	Transient Temperature Analysis of a Small Slab - A Comparison of Mathematical and Approximate Methods of Analysis - Total Slab Thickness = 0.05 Inch	34
11	Thermal Conductance and Capacity of Small Slabs Used in an Approximate Method of Analysis	35
12	An Illustration of the Deviation of the Approximate Method From the Mathematical Method of Analysis of a Small Slab Subjected to Sudden Heating or Cooling	36
13	Temperature Variation of the Relaxation Time of Polycrystalline Al_2O_3	37
14	An Infinite Matrix of Square Cooling Channels in a Heat Generating Medium	38
15	A Map of the Stress Function in a Square Unit Cell	39
16	A Map of the Stresses in a Square Unit Cell	40

FIGURES

		Page
17	Thermal Stress Distribution in the Wall of a Square Unit Cell in an Infinite Matrix of Cells	41
18	Heat Generation and Calculated Temperatures in a Unit Cell	42
19	Calculated Maximum Tangential Thermal Stresses in a Unit Cell	43
20	Calculated Tangential Thermal Stresses In the Perforated Cylinder	44
21	Combined Cylinder and Unit Cell Viscoelastic Tangential Thermal Stresses	45

BIBLIOGRAPHY 46

APPENDIX A

Determination of the Instability of the Finite Difference Equations for Heat Conduction in a Unit Cell 47

APPENDIX B

Derivation of an Approximate Method of Determining the Transient Temperature Distributions in a Unit Cell and a Comparison with a Mathematical Solution 50

APPENDIX C

Heat Transfer in Perforated Geometries with Volumetric Heat Dissipation and Volumetric Heat Generation 61

APPENDIX D

Derivation of the Thermal Stress Equations for a Maxwell Cylinder Based on the Elastic Viscoelastic Analogy 64

APPENDIX E

The Boundary Conditions for Thermal Stress in a Unit Cell in a Perforated Geometry 69

Page

APPENDIX F

Solution of the Inelastic Thermal Stress Equations for the Unit Cell and Parent Cylinder by Numerical Methods and the Determination of the Stability Requirements 82

NOMENCLATURE 90

TRANSIENT TEMPERATURES AND INELASTIC THERMAL STRESSES IN GAS-COOLED PERFORATED CERAMIC CYLINDERS WITH INTERNAL HEAT GENERATION

INTRODUCTION

The purpose of this report is to present a method for estimating the transient temperature distributions and inelastic thermal stresses in perforated, cooled ceramic cylinders with internal heat generation. The determination of the inelastic thermal stresses is based on the elastic viscoelastic analogy (1, p. 578-595; 4, p. 105). The analysis of thermal stresses in perforated geometries is based, with some latitude, on the method of G. Horvay (6, p. 355-360). The heat transfer process in the perforated, cooled cylinder is based on the concept of volumetric heat dissipation. Several appendices to the report contain detailed derivations and explanations that serve as a complete development of the method presented. Some results of a study using the method described are presented as an example of its use.

1. Heat Transfer

a. Unit Cells

A unit cell is defined as a coolant hole in a perforated cylinder surrounded by ceramic whose outer boundary is defined by lines of symmetry (see Figure 1). For ease of analysis, the small unit cell is converted to an equivalent hollow cylinder cross section. A sketch of a typical perforated ceramic cylinder is shown in Figure 1.

To demonstrate the use of the analytical method outlined in this report, a helium-cooled aluminum oxide cylinder was analyzed (Figure 2). This cylinder has a void fraction of 0.5 representing 140 cooling channels. These cooling channels have an inner radius, a, of 0.299 inch and the outer radius, b, of the unit cell model is 0.423 inch. The radius of the cylinder is 5.0 inches. The helium flow in each channel is 0.1 lb/sec at a constant temperature of 1500° F. The outer boundary of the cylinder is kept at 1500° F.

In the transient heat transfer analysis of the unit cell, a finite difference solution of the differential equation must be used since physical properties, power generation, ambient conditions, etc., may be changing with time. The stability of the finite difference equations depends upon the compatibility of the unit cell dimensions, thermal properties and time increment chosen. This poses

a tremendous problem immediately in the analysis since the small dimensions of the unit cell model and the thermal properties of the material (see Figure 3) force the use of an extremely small time increment to maintain equation stability.

The differential system which describes the heat transfer process in a unit cell is

$$\frac{\partial^2 T}{\partial r^2} + \frac{1}{r}\frac{\partial T}{\partial r} + \frac{q_v}{k} = \frac{\rho c}{k}\frac{\partial T}{\partial t} \qquad (1)$$

(1) $\frac{\partial T}{\partial r} = 0$ at $r = b,\ t = t$

(2) $k\frac{\partial T}{\partial r} = h(T - T_0)$ at $r = a,\ t = t$

(3) $T = T_i$ at $r = r,\ t = 0.$

The finite difference representation of this system and the determination of the stability criteria are given in Appendix A. A plot of the stability factor as a function of time of operation for the equations for a unit cell is presented in Figure 4. The temperatures at which the thermal properties were evaluated are presented in Figure 5. The base lines labeled "boundary" and "interior" in Figure 4 represent the values of stability factor below which the respective equations would be unstable.

It may be seen from Figures 4 and 5 that the selection of a time interval which will maintain system stability over a wide range of temperatures is not an easy

matter. Even during the period of highest operating temperature the time interval would be less than 0.5 second. At lower operating temperatures the time interval is much less than 0.25 second. This makes hand computation time consuming and high speed machine computation costly.

The first problem encountered then was to determine the transient temperature distributions in a unit cell during a desired operating period. Since the usual methods of analysis, i.e., the mathematical and the numerical representation of the mathematical, were ruled out on the grounds of complexity and impracticability, an approximate method was devised. This method is based upon the consideration of the unit cell model as one region, i.e., all heat is transferred, absorbed and generated at one radial position in the model (in this case, the outer periphery of the model). The basic equation of the approximate method is:

$$\rho c V \frac{dT_{max}}{dt} = q_v V - 2\pi a U (T_{max} - T) dx \qquad (2)$$

where

$\rho c V \frac{dT_{max}}{dt}$ = Heat storage

$q_v V$ = Heat generation

$2\pi a U (T_{max} - T) dx$ = Heat transfer.

A further approximation is made with regard to the temperature distribution within the unit cell model wall. In the one region model considered, the temperature distribution within the wall is due only to the heat transfer term in Equation (2) since the storage and generation of heat occurs at the outer boundary only. This heat flow would produce the usual steady-state temperature distribution for a hollow cylinder without heat generation. In the actual case, heat storage and generation, distributed in some manner over the unit cell radius, will not produce this type of temperature distribution. A simple approximation of the correct temperature distribution may be made by considering the heat transferred in the unit cell wall as volumetric heat generation, distributed uniformly, to be used in the steady-state form of the differential system (1). This was found to be a fair approximation provided the unit cell wall thickness does not exceed about 0.15 inch (see Figure 6). This conclusion was based upon a comparison with a classical mathematical solution to the problem (see Appendix B and Figures 7 through 10). A more detailed account of the approximate methods discussed here are presented in Appendix B. It must be pointed out at this time that the approximate method discussed cannot evaluate sudden heating or cooling such as in quenching, etc., where a sudden reversal of the slope

of the temperature profile is experienced. A typical example of such a situation is shown in Figure 12. The temperature distributions that might be obtained by the approximate method are shown by dotted lines in Figure 12. A reversal of the slope of the temperature profile such as that shown would not be experienced by the unit cell under carefully controlled conditions. At steady coolant conditions power changes would not produce the reversal of slope shown and changes in coolant conditions could be carefully controlled to avoid such a situation.

b. Parent Cylinder

The heat transfer process in the perforated, cooled cylinder (see Figures 1 and 2) is defined by the equation:

$$k\nabla^2 T - U_v (T-T_0) + q_v = \rho c \frac{\partial T}{\partial t} \qquad (3)$$

where

$k\nabla^2 T$ = the conduction term

$U_v (T-T_0)$ = a term for dissipation due to multiple sinks

q_v = the internal heat generation term

$\rho c \frac{\partial T}{\partial t}$ = the storage term.

In this type of geometry, the heat transfer by conduction through the perforated mass is hampered by the perforations which, when cooled, provide for heat dissipation. If the object is of moderate dimensions, is cooled or heated at the outer periphery and has many small cooling channels representing a substantial void fraction, an analysis of individual isolated unit cells will not provide a reasonable estimation of the heat transfer process in the object. A reasonable estimation of the heat transfer process may be obtained by the use of Equation (3) with an "apparent" thermal conductivity, k, and a "volumetric heat dissipation coefficient", U_V. The terms k and U_V are functions of the void fraction of the object. The defining equations for these terms are presented in Appendix C.

There are limitations on the validity of this treatment which have not been established. The limitations of this treatment will depend upon a parameter relating cooling passage diameter, void fraction, number of cooling passages and overall dimensions of the perforated object. For example, it is possible to have two objects with the same overall dimensions and void fraction, however, one could have several cooling passages of small diameter while the other could have one large cooling passage (e.g., a hollow cylinder). The latter object

could not be analyzed using Equation (3). The limitations of the method could be established by experiments which would evaluate the parameter mentioned. This parameter could then be used in the same manner as Reynolds number is used for fluid flow problems, i.e., to establish a valid range of usefulness of the method for any situation.

2. Thermal Stress

a. Viscoelastic Theory

The inelastic thermal stresses dealt with in this report are based upon the elastic viscoelastic analogy for a material with creep (Maxwell body). This is the simplest idealization of the mechanical behavior of structural materials at elevated temperatures. An excellent discussion of the theory of inelastic stress is given by A. M. Freudenthal (1, p. 578-595; 4, p. 205) which is the basis for the inelastic thermal stress work presented in this report. My derivation of the equations for radial (σ_r) and tangential (σ_θ) thermal stresses in a Maxwell cylinder, based upon the elastic viscoelastic analogy, is presented in Appendix D. The derivation in Appendix D yields two simultaneous partial differential equations for σ_r and σ_θ that can be separated only by the assumption of an incompressible medium. This assumption manifests itself as a Poisson's ratio of 0.5 for the material under study.

Any transient thermal stress study based upon the elastic viscoelastic analogy is heavily dependent upon the relaxation time τ of the material. The relaxation time is defined by the relationship:

$$\tau = \frac{\eta}{G} \qquad \text{(1, p. 579)} \qquad (4)$$

where

η = material viscosity

G = material modulus of rigidity

The temperature dependence of τ is primarily due to the temperature dependence of η which may be expressed as

$$\eta = \eta_0 \exp\left[\frac{Q}{RT_0}\left(\frac{T_0}{T} - 1\right)\right] \qquad \text{(1, p. 578)} \qquad (5)$$

where

Q = activation energy

R = the universal gas constant

T = absolute temperature

T_o = reference absolute temperature

η_o = reference viscosity at T_o

Therefore, neglecting changes in the modulus of rigidity

$$\tau = \tau_0 \exp\left[\frac{Q}{RT_0}\left(\frac{T_0}{T} - 1\right)\right] \qquad (6)$$

where

τ_o = reference relaxation time at T_o.

For the aluminum oxide cylinder of Figure 2 the reference relaxation time was estimated from internal friction data for polycrystalline Al_2O_3 (2, p. 21). According to Chang (3) if we use the frequency and the temperature at which the peak occurs on the internal friction plot, we can approximate τ_o in the following manner:

$$\tau_o = \frac{1}{2\pi f_o} \tag{7}$$

where

f_o = frequency producing peak internal friction at T_o.

Chang points out, however, that this implies stress relaxation by the mechanism of grain boundary slip over the entire temperature range considered where, in reality, other mechanisms may be predominant at high temperatures.

A plot of the temperature variation of the relaxation time for polycrystalline Al_2O_3 (based on equations 6 and 7) is presented as Figure 13.

b. Thermal Stresses in Perforated Geometries

According to Horvay (6, p. 355-360) a thermal stress analysis can be made for a perforated plate by using the usual thermal stress equations with the elastic modulus E and Poisson's Ratio μ for the solid material replaced by modified values for the perforated material. The modified E and μ are functions of the web thickness to radius

ratio for the unit cell. As pointed out in section 2a, page 8, concerning viscoelastic theory, a Poisson's ratio of 0.5 must be assumed, consequently, no modification of μ is necessary. However, the value of E used in the analysis of the perforated cylinder of Figure 2 was modified according to Horvay's suggestion. Horvay also suggests modifying the thermal conductivity k of the material by multiplying by the web thickness to radius ratio for the unit cell. This modification of k was not used in favor of one proposed by Jakob (7, p. 85) which is given as Equation (C-2) in Appendix C. In discussing the limitations of his method of analysis Horvay emphasizes the fact that the temperature distribution must not vary by more than infinitesimal amounts from hole to hole. In this respect the method of Horvay is used with great latitude since substantial variations in temperature from hole to hole are encountered in many situations to which the method outlined in this report is applied.

When computing the elastic thermal stresses in a perforated geometry the thermal stresses in the parent element due to the variation in temperature across the holes are superimposed upon the thermal stresses calculated for the unit cell due to the temperature variation across the web. This procedure is suggested by Horvay (5, p. 18).

The viscoelastic thermal stresses in a body are extremely sensitive to the environment. Any forces imposed, even momentarily, during the operating history of the body may affect the final stress level attained. Consequently, any superposition of the thermal stresses in the unit cell and the parent perforated geometry should be done at the time computed before proceeding to the next time in order to account for the interaction. This instantaneous superposition of the stresses represents a rather formidable computational task at this time. In this report the stresses in the unit cell and parent geometry are computed separately and combined at the end of the computations.

c. Boundary Conditions for Thermal Stresses in a Unit Cell

One of the most perplexing and controversial areas encountered in the pursuit of the subject of thermal stresses in perforated geometries was that of the boundary conditions of the unit cell. At first it was assumed that an equivalent cylinder model of a unit cell could be treated as an isolated cylinder with no normal forces at the inner and outer surfaces (i.e., zero radial stresses at the surfaces). However, it seemed more logical that a condition of symmetry would exist at the outer boundary of a unit cell in a sufficiently large cluster of identical unit cells. This latter approach was taken only to find

that the summation of the moments obtained in the unit cell was not zero. Although this could be explained analytically, it did not seem to be a realistic representation of the actual situation. In order to provide some indication of the actual conditions which would exist, a simple infinite matrix of square unit cells with square cooling channels (see Figure 14) was analyzed by setting up a network of nodes for the finite difference representation of the biharmonic equation. The results of this study (Figures 15, 16 and 17) indicate that conditions of symmetry do exist at the outer boundary of a square unit cell, however, the magnitude and distribution of those stresses comparable to the tangential stresses in a hollow cylinder are similar to those of a hollow cylinder with zero radial stresses at the surfaces (see Figure 17). In order to provide a complete picture of the study made both analytical approaches mentioned are presented in Appendix E.

d. Transient Unit Cell Temperature Representation in the Thermal Stress Equation

In the partial differential equation for the elastic viscoelastic radial stress in the equivalent cylinder model of a unit cell (see Equation F-1, Appendix F) a temperature-time derivative ($\frac{\partial^2 T}{\partial r \partial t}$) exists on the right hand side of the equation. The question arises, considering the approximation discussed in section 1a, page 2, and

in Appendix B, how this time-temperature differential is obtained. The answer to this question lies in another approximation based upon the first. This compounding of approximations is an unfortunate necessity in this particular study, however, the error involved is predominantly that discussed in Appendix B and illustrated in Figures 6 through 10. A detailed development of the time variable approximation of the temperature gradient ($\frac{\partial^2 T}{\partial r \partial t}$) is presented in Appendix F.

3. Method of Analysis

The discussion of the heat transfer and thermal stress theory of the preceding sections, with the numerous references to the appropriate appendices, outlines the general approach to the analysis of perforated gas-cooled geometries with internal heat generation. The purpose of this section is to present a specific analytical procedure based upon equations extracted from the many theoretical derivations and their associated approximations.

Step 1: Heat Transfer in the Perforated Cylinder

The temperature distributions (maximum unit cell temperatures) in the perforated cylinder and the heat dissipation to the cooling holes are determined in this step.

Equation (C-1) (Appendix C) is solved by numerical methods to yield the temperature distributions in the cylinder at various times. The volumetric heat dissipation

coefficient, defined by Equation (C-9), is evaluated by first using Equation (B-8) for the overall heat transfer coefficient for the unit cell. The heat dissipated to a cooling hole may be calculated by Equation (C-5).

The heat transfer boundary conditions for the perforated cylinder of Figures 1 and 2 are:

(1) $\frac{\partial T}{\partial R} = 0$ at R = O

(2) T = O at R = A

(3) $T = T_i$ at t = time = O.

Step 2: Thermal Stresses in the Perforated Cylinder

The distributions of radial thermal stress in the perforated cylinder are calculated by Equation (F-29). The term $\frac{\Delta}{\Delta t}\left(\frac{\Delta T}{\Delta R}\right)$ is obtained from the results of Step 1. The tangential thermal stresses are the highest stresses in the cylinder and are obtained from Equation (F-35) once the radial stresses are known.

The thermal stress boundary conditions for the perforated cylinder of Figures 1 and 2 are:

(1) $\frac{\partial \sigma_R}{\partial R} = 0$ at R = o

(2) $\sigma_R = 0$ at R = A

(3) $\sigma_R = \sigma_R$(initial) at t = o.

Elastic thermal stresses may be obtained by using an infinite relaxation time in Equation (F-29).

Step 3: Heat Transfer in the Unit Cell

The temperature distributions in the unit cell are obtained from Equation (B-7). Before this equation can be used, the maximum unit cell temperature and the heat dissipation to the coolant channel must be obtained from Step 1. The fictitious value of heat generation for the unit cell is derived from the heat dissipation according to Equation (B-6).

Step 4: Thermal Stresses in the Unit Cell

The highest thermal stresses in the unit cell model are the tangential stresses. These stresses are determined from Equation (F-18). For this equation, $\mathcal{F}_a$ is defined by Equation (F-16) and (F-17) and τ_n is found from the procedure outlined in section 2a, page 8. The term $\left(\frac{q_{v,n+1}}{k_{n+1}} - \frac{q_{v,n}}{k_n}\right)\frac{}{\Delta t}$ is obtained from the results of the unit cell heat transfer analysis of Step 3 (see Equations F-1 through F-18).

The thermal stress boundary conditions for the unit cell model for the perforated cylinder of Figures 1 and 2 are:

(1) $\sigma_r = 0$ at r = b

(2) $\sigma_r = 0$ at r = a

(3) $\sigma_r = \sigma_r$(initial) at $t = t_i$.

Elastic thermal stresses may be obtained by using an infinite relaxation time in Equation (F-18).

Step 5: Combination of Unit Cell and Cylinder Thermal Stresses

The final step in the analytical procedure is the combining of the tangential thermal stress in the perforated cylinder with the maximum tangential thermal stress in a unit cell at the same radial location in the perforated cylinder.

To demonstrate the use of the analytical method presented in this report, the helium-cooled aluminum oxide cylinder of Figure 2 was analyzed.

When subjected to the power schedule of Figure 18 and the other conditions already mentioned (Figure 2), the maximum temperature in a unit cell (calculated by the methods outlined) will vary in the manner shown in Figure 18. The conditions which cause this variation in maximum unit cell temperature also produce severe elastic tangential thermal stresses in the unit cell (see Figure 19). The allowable tensile stress for aluminum oxide at 2000° F is 32,500 psi. At 1800° F the stresses calculated using the viscoelastic equations depart from the elastic curve at about 30,000 psi, peak at about 31,000 psi and then drop sharply. The second peak on the viscoelastic curve of Figure 19 is due to an arbitrary change in the relaxation time. At this point, the temperature dependence of τ was abandoned in favor of a constant value of 5.0 seconds. This was necessary since the time interval of computation in this demonstration was 5.0 seconds and the stability factor for the equations used did not permit a value of τ less than 5.0 seconds. In actual practice, high speed computing machines would eliminate this restriction. The third peak on this curve occurs where τ exceeds 5.0 seconds due to a reduction of the temperature.

A similar curve (Figure 20) was generated for the tangential thermal stresses in the perforated cylinder at a point on the radius corresponding to the location of the unit cell. As the final step in the analysis, the viscoelastic thermal stresses in the unit cell and the perforated cylinder are combined to give the total predicted maximum thermal stresses in the cylinder (see Figure 21).

The results plotted in Figures 19, 20 and 21 represent only a portion of the complete results obtained in this study. Many similar plots could have been prepared for other locations in the perforated cylinder, however, those presented are typical and serve to illustrate the advantages of determining thermal stresses using inelastic theory.

The viscoelastic thermal stresses in a body are sensitive to the environment. Any forces imposed, even momentarily, during the operating history of the body may affect the final stress level attained. Any superposition of the thermal stresses in the unit cell and the parent perforated geometry should be done at the time computed before proceeding to the next time increment in order to account for the interaction. This superposition of the stresses represents a rather formidable computational task at the present time. To simplify the computations for the

example given in this paper, superposition of the stresses was the final step in the analysis.

The elastic stresses of Figures 19, 20, and 21 would go to zero as the temperature of the cylinder reaches a uniform value of 1500° F at the end of the operating period, however, the viscoelastic stresses would not go to zero. There are "frozen in" compressive stresses present due to the inelastic behavior of the material. These "frozen in" stresses would be the initial stresses in the cylinder for any subsequent operating procedure. Repeated cycling according to the schedule described would result in a moderate build-up of the compressive stresses which would eventually level off to a nearly constant value. Excessive cycling, however, could result in failure due to fatigue.

The method presented in this report should provide a way of estimating thermal stresses in perforated geometries during transient operation and should serve to provide some insight to the phenomena associated with high temperature operation. The approximations used in some phases of the method do not place it in the highly rigorous category required for exacting research investigations, however, it does provide a means of analysis of a difficult situation where there previously was none. It is recommended that the techniques presented here be checked by suitable experiments to establish the range of usefulness, errors involved, etc.

An unfortunate limitation of the method presented is its inability to evaluate temperature and thermal stress distributions for sudden heating and cooling such as in quenching, etc., where a sudden reversal of the slope of the temperature profile in the unit cell wall is experienced. This limitation, however, should not detract from the value of the method for the prediction of temperatures and thermal stresses in a controlled environment or for establishing such an environment.

The approximation of the temperature distribution in the unit cell wall (see section 1a, page 2) was found to be within about 5 percent of the temperature distribution

obtained by more rigorous methods, provided the unit cell wall thickness does not exceed about 0.15 inch (see Figure 6).

From the analysis of the infinite matrix of square cooling channels in a heat generating medium (see Figure 14 (a) and Appendix E), it was concluded that the boundary conditions for radial thermal stress in the unit cell model of Figure 1 should be zero radial stress at the inner and outer radii. Although a condition of symmetry was obtained in the analysis of Appendix E, the resultant stresses, comparable to the tangential stresses in the unit cell model, were distributed in a manner suggesting stress-free boundaries.

The greatest single factor affecting the prediction of the transient inelastic thermal stresses in materials operating at high temperature is the relaxation time. This property is not available for aluminum oxide and other data from which it might be predicted are not readily available. The method used in this report to obtain the relaxation time implies that stress relaxation occurs by the mechanism of grain boundary slip where, in reality, other mechanisms may be predominant at high temperatures. The results presented in Figures 19 and 20 suggest that, in aluminum oxide, creep starts at about 1800° F. The

validity of the method used for obtaining relaxation time might be related to this point of departure from the elastic curve.

The phenomenon of "frozen in" stresses discussed on page 20 suggests one possible use of the analytical method presented in this report. The process for making ceramic objects includes a period of "firing" at high temperatures to bring about fusion. Upon cooling, these ceramic objects may have "frozen in" stresses which could cause premature failure depending upon the conditions to which the object is subjected. The analytical method of this report could be used to devise an annealing process for controlling the "frozen in" stresses of ceramics to eliminate weaknesses or, possibly, to provide "built-in" strength.

Figure 1. PERFORATED COOLED CYLINDER

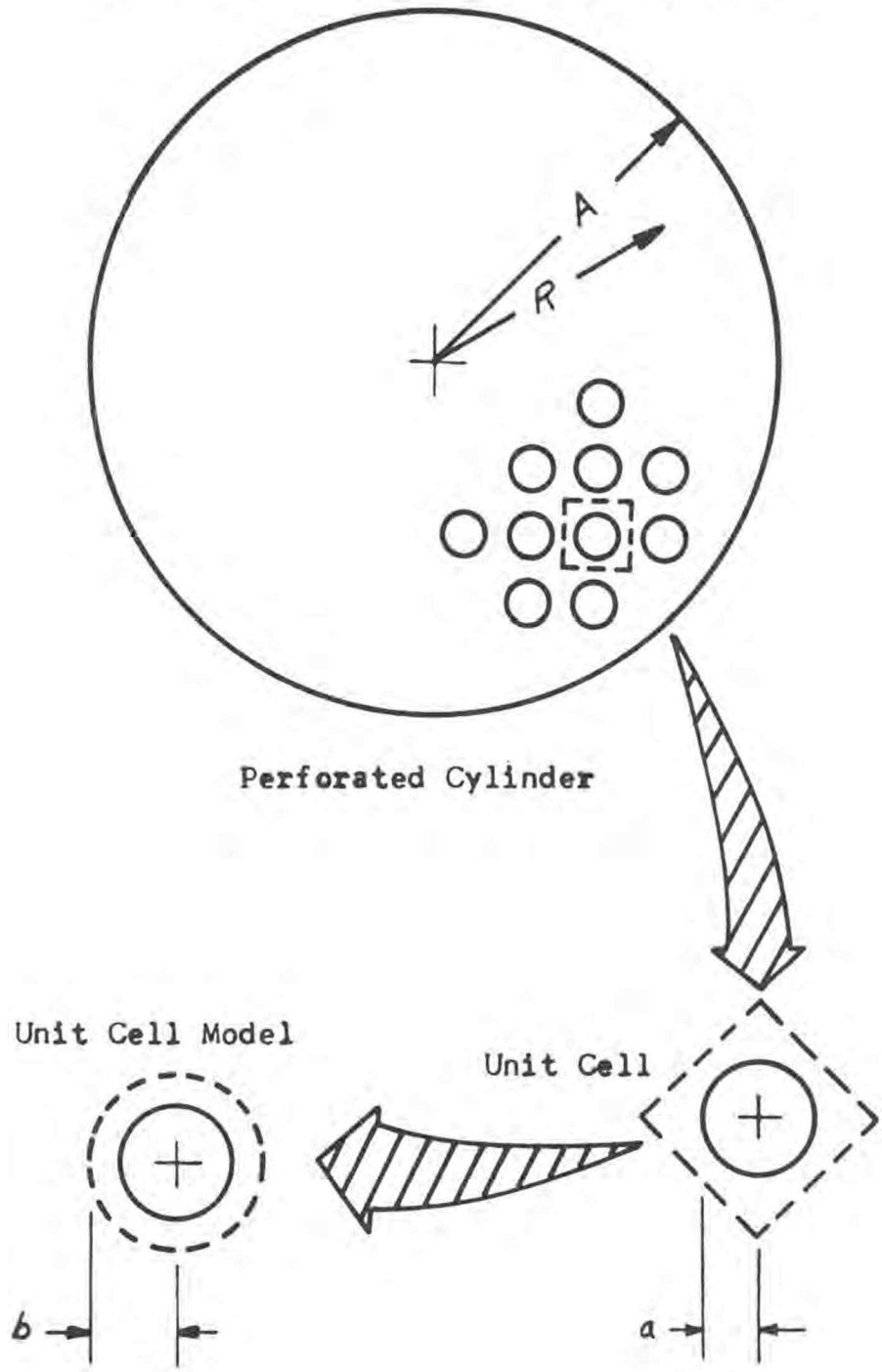

Figure 2. ALUMINUM OXIDE CYLINDER

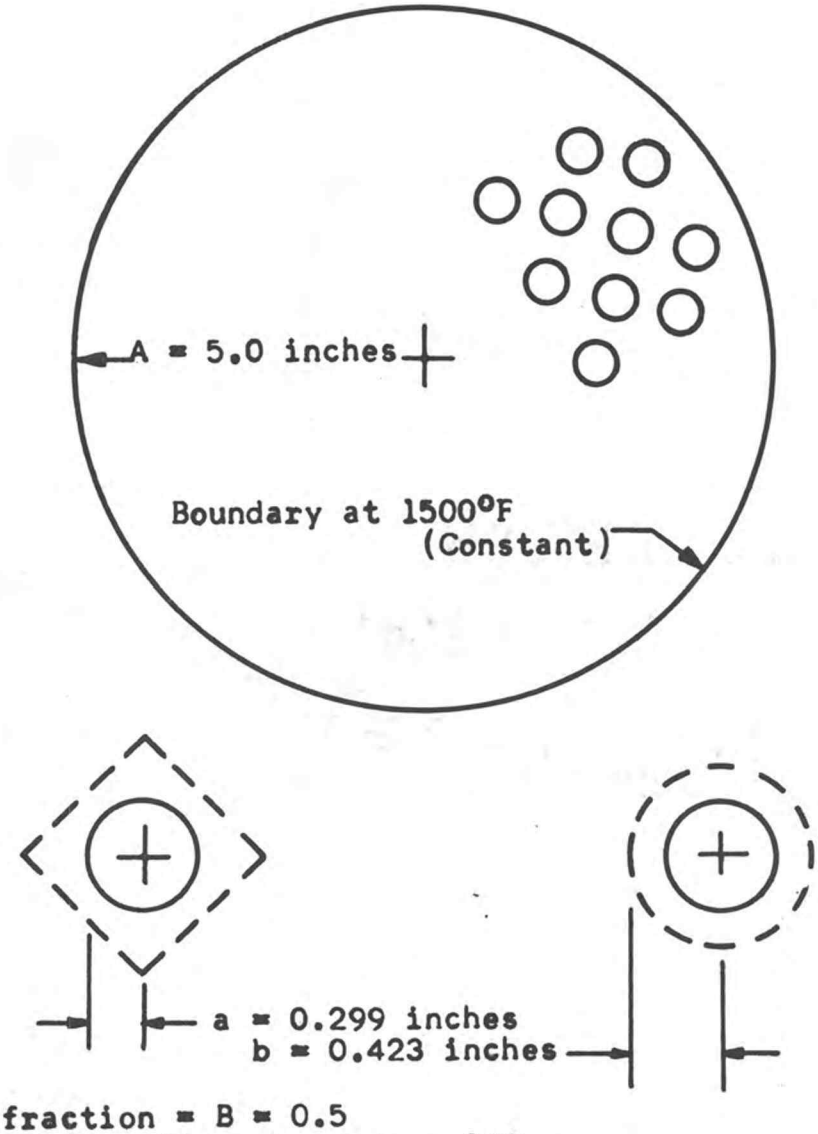

Void fraction = B = 0.5
Number of cooling channels = 140
Helium cooled: T (Gas) = 1500°F (Constant)
W = Flow rate per channel
= 0.1 lb/secxchannel
Property data: Density = 3.8 gm/cc
E_o = 5.3×10^7 psi
α^o = 4.45×10^{-6} in/inx°F

Figure 3. THERMAL CONDUCTIVITY AND OTHER PROPERTY DATA FOR ALUMINUM OXIDE

Heat capacity = 0.23 B/lb°F

Density = 0.137 lb/in^3

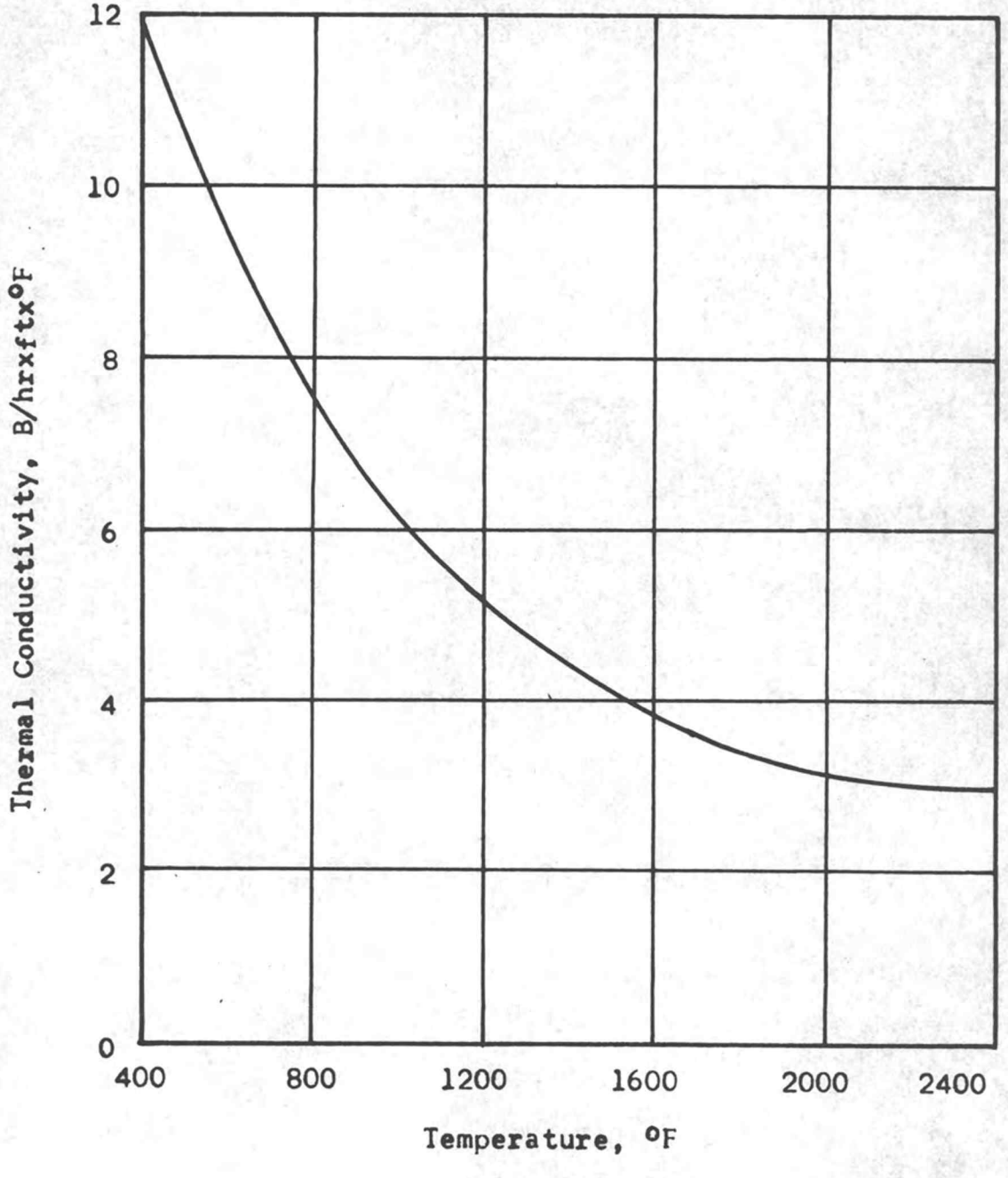

Figure 4. STABILITY OF THE FINITE DIFFERENCE APPROXIMATION OF THE UNIT CELL HEAT TRANSFER EQUATION

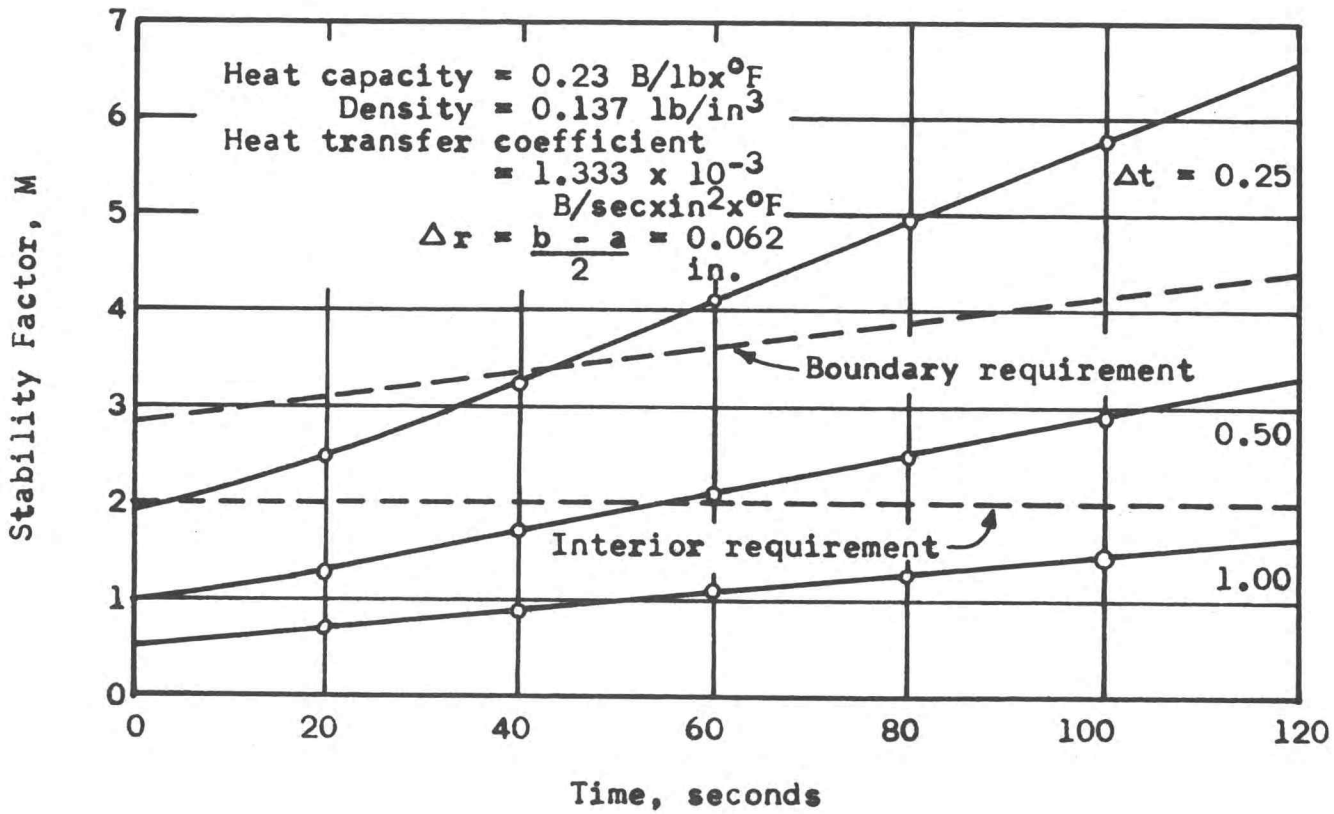

Figure 5. TEMPERATURES USED IN THE EVALUATION OF THE STABILITY OF THE FINITE DIFFERENCE APPROXIMATION OF THE UNIT CELL HEAT TRANSFER EQUATION

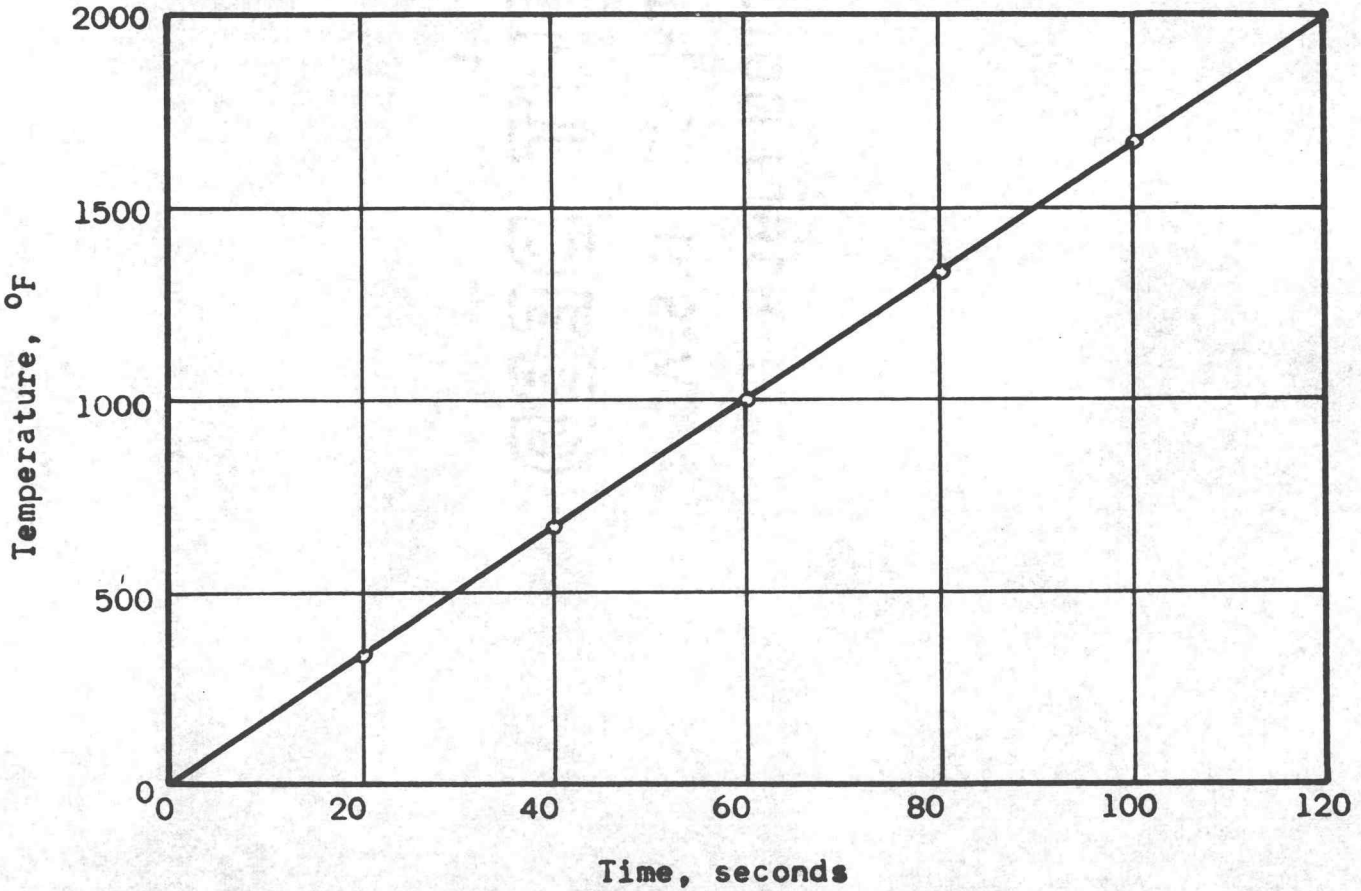

TABLE I

TRANSIENT TEMPERATURES IN SLABS OF VARIOUS THICKNESSES WITHOUT HEAT GENERATION - A COMPARISON OF MATHEMATICAL AND APPROXIMATE METHODS OF CALCULATION

Slab Thickness (inches)	Temperature at 3.0 Seconds, °F				Percent Deviation of Approximate Method from Mathematical Method	
	Mathematical Method		Approximate Method			
	Interior	Surface	Interior	Surface	Interior	Surface
0.6	104	574	171	683	-64.4	-19.0
0.3	200	576	288	606	-44.0	- 5.2
0.1	669	741	671	740	- 0.3	0.1
0.05	908	920	904	915	0.4	0.5

Figure 6. TRANSIENT TEMPERATURE ANALYSIS OF A SMALL SLAB

A comparison of mathematical and approximate methods of analysis at 3.0 seconds after start of heating.

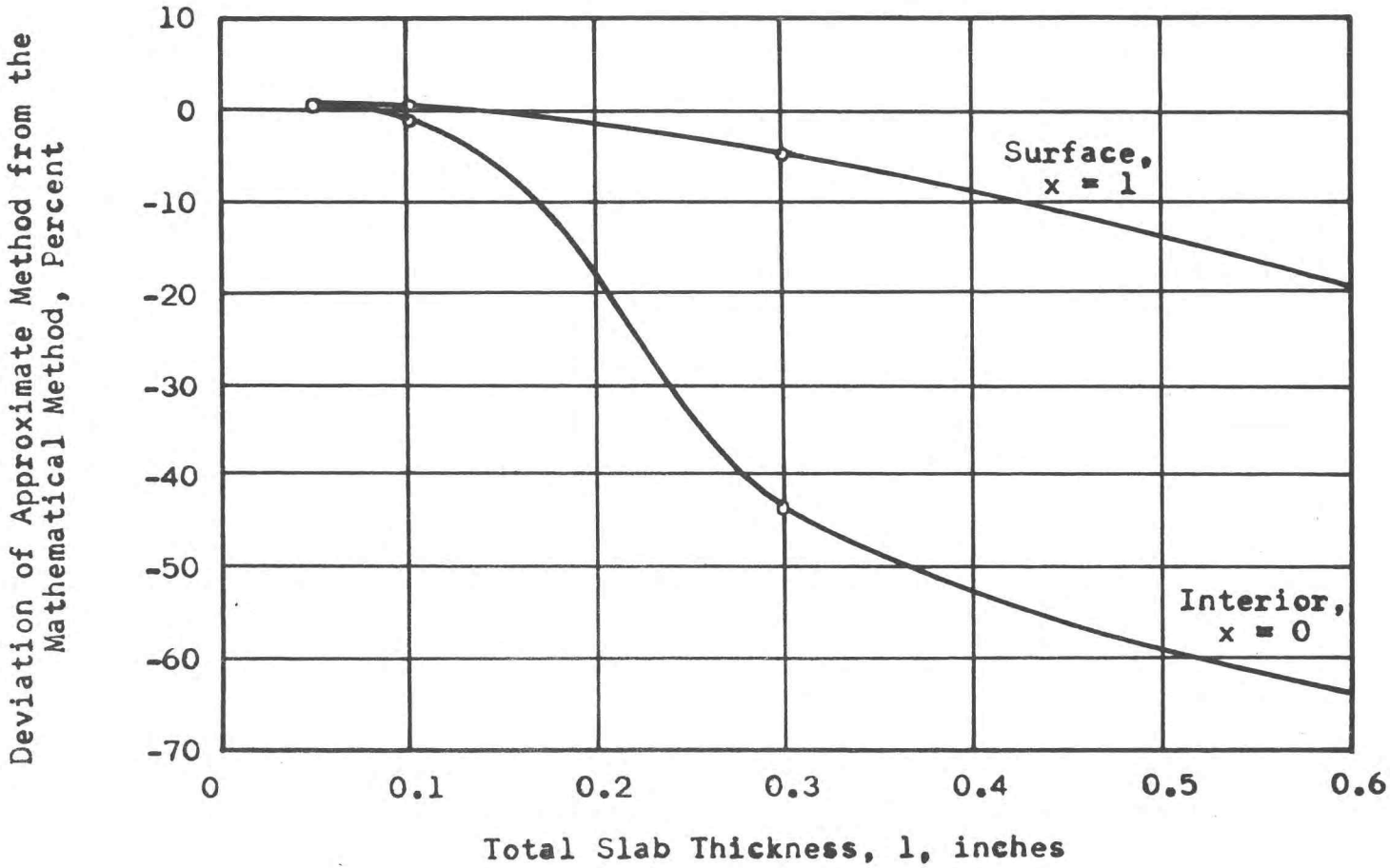

Figure 7. TRANSIENT TEMPERATURE ANALYSIS OF A SMALL SLAB

A comparison of mathematical and approximate methods of analysis at 3.0 seconds after start of heating. Total slab thickness = 0.6 inch.

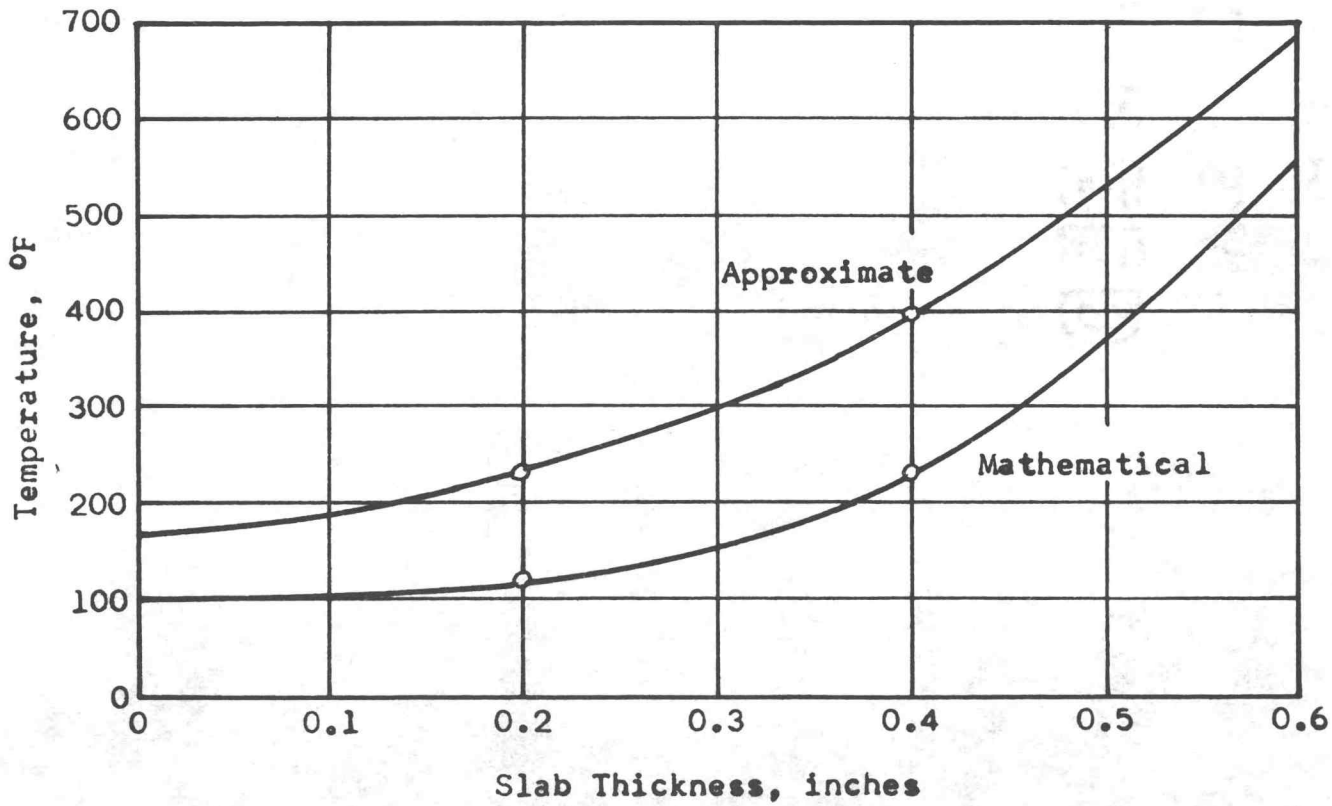

Figure 8. TRANSIENT TEMPERATURE ANALYSIS OF A SMALL SLAB

A comparison of mathematical and approximate methods of analysis at 3.0 seconds after start of heating. Total slab thickness = 0.3 inch.

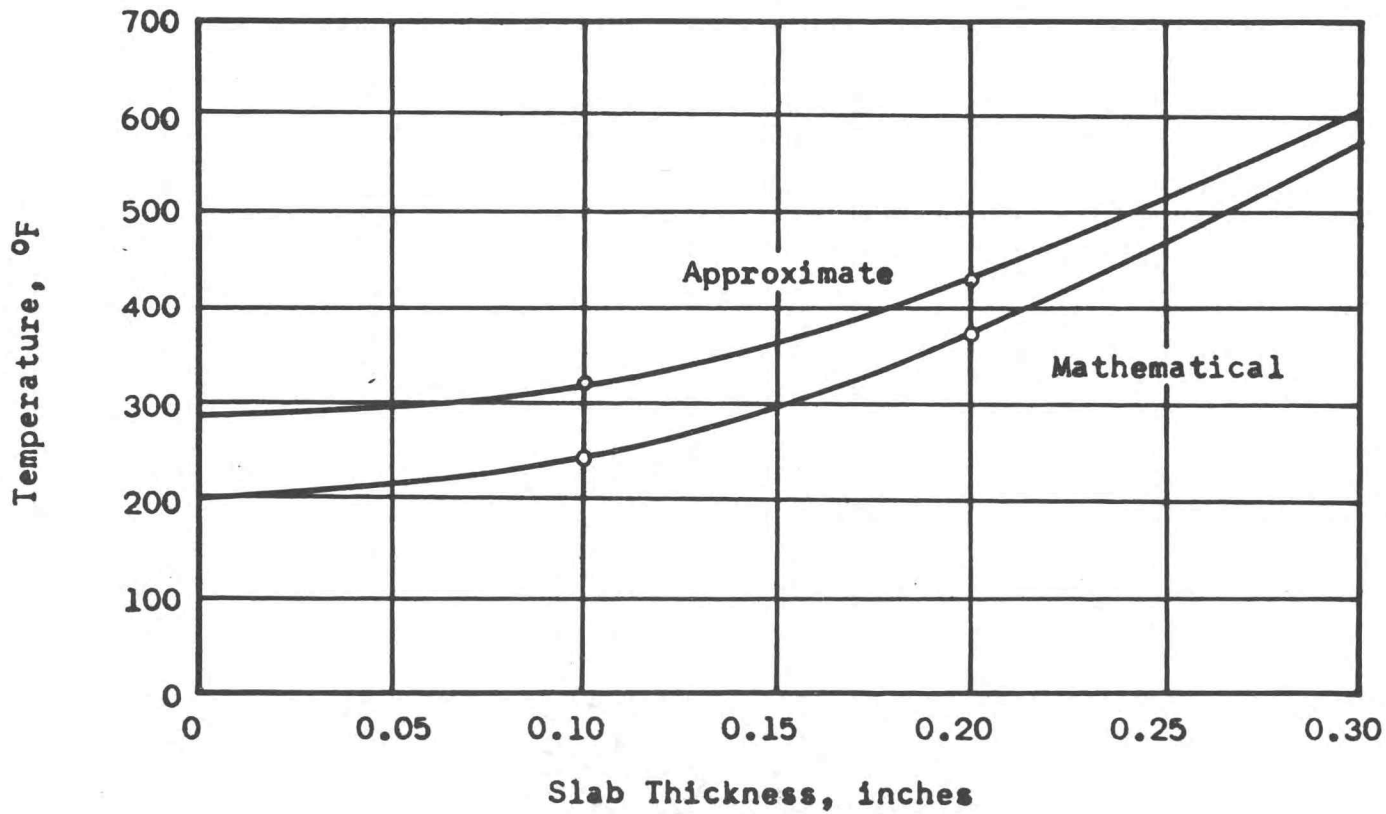

Figure 9. TRANSIENT TEMPERATURE ANALYSIS OF A SMALL SLAB

A comparison of mathematical and approximate methods of analysis at 3.0 seconds after start of heating. Total slab thickness = 0.1 inch.

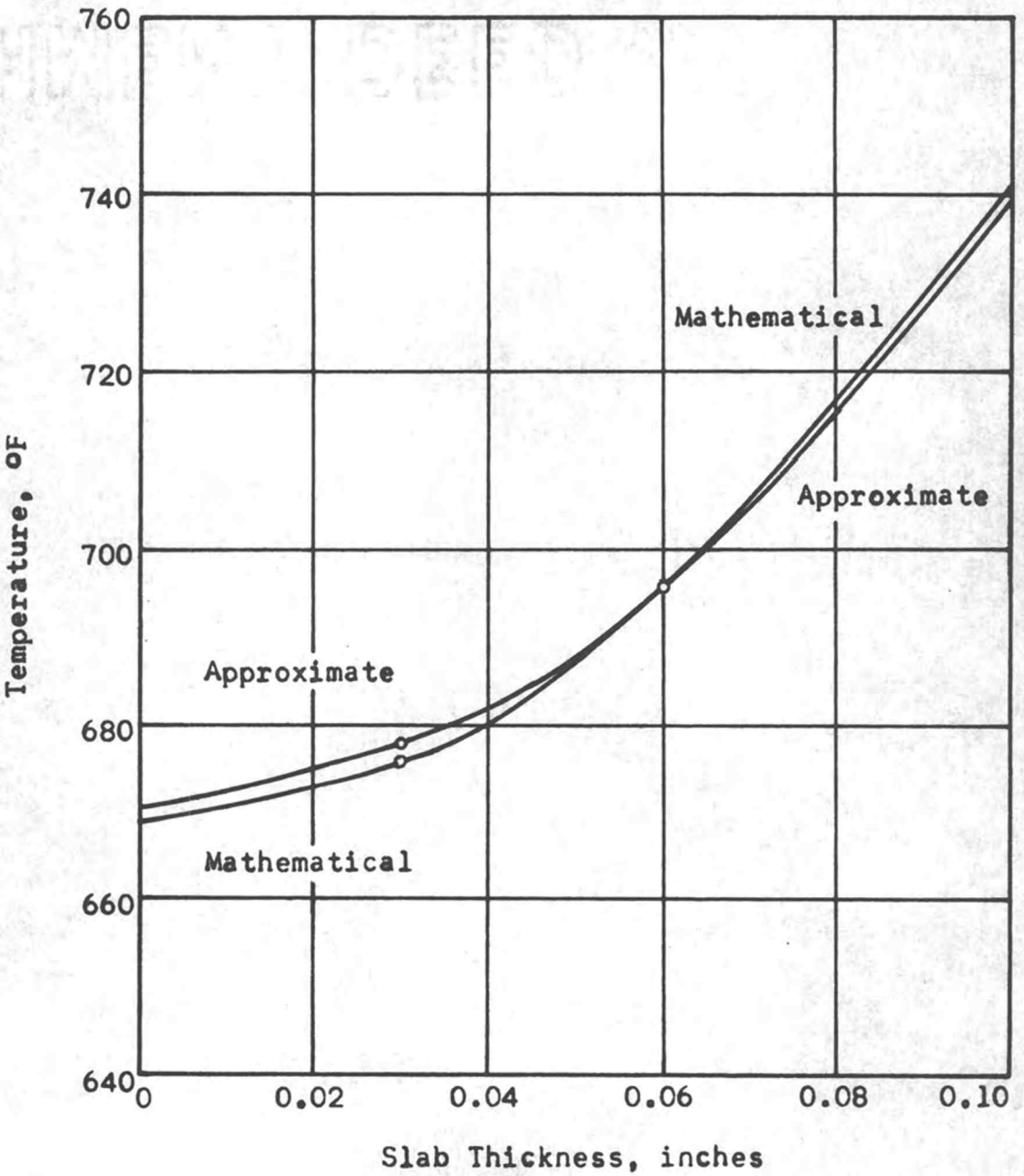

Figure 10. TRANSIENT TEMPERATURE ANALYSIS OF A SMALL SLAB

A comparison of mathematical and approximate methods of analysis at 3.0 seconds after start of heating. Total slab thickness = 0.05 inch.

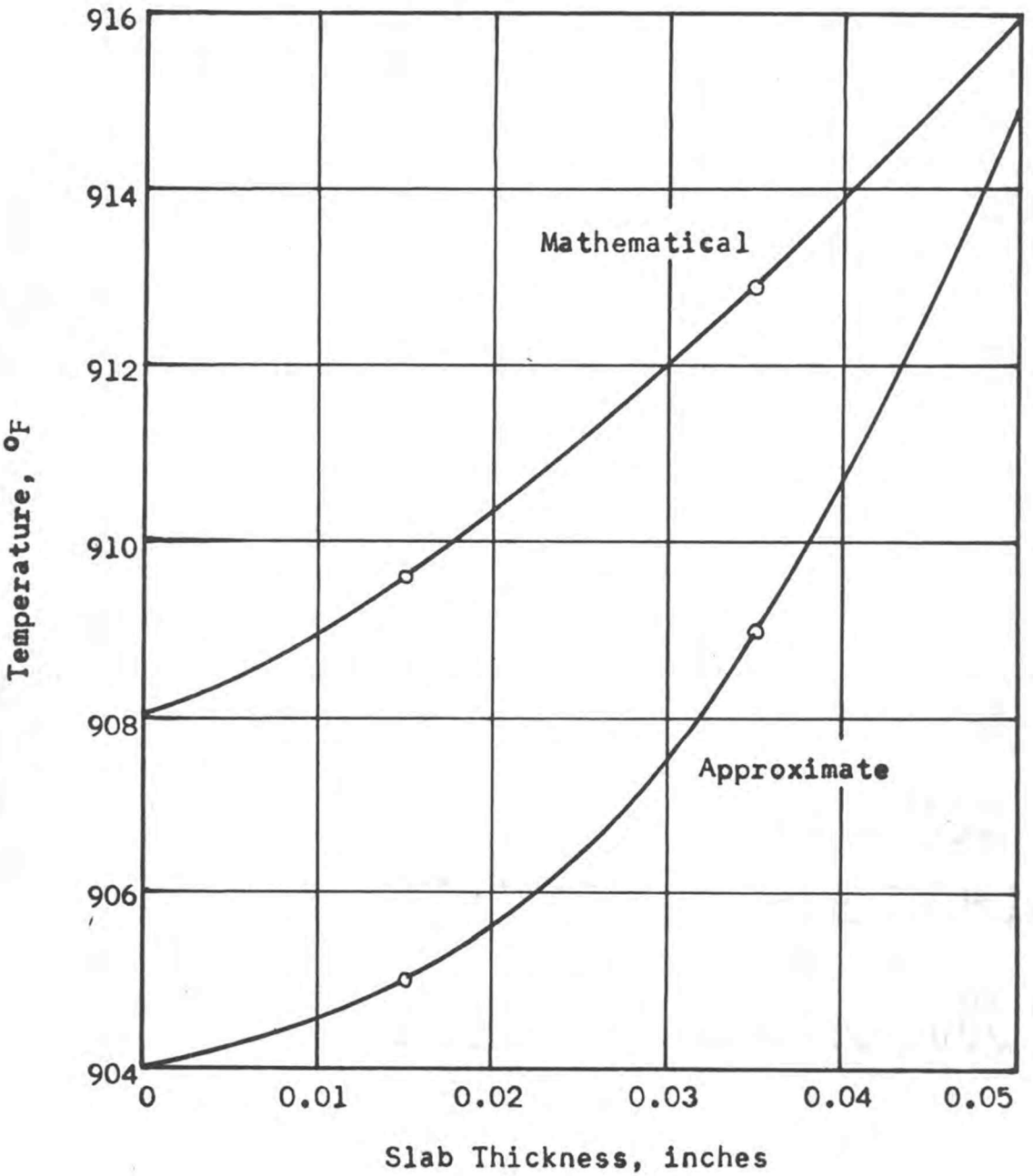

Figure 11. THERMAL CONDUCTANCE AND CAPACITY OF SMALL SLABS USED IN AN APPROXIMATE METHOD OF ANALYSIS

Aluminum oxide heated by helium at 1000°F.

$\rho = 0.137$ lb/in^3
C = 0.23 B/lbx°F
k = 2.48×10^{-4} B/secxinx°F
h = 1.333×10^{-3} B/secxin^{2}x°F

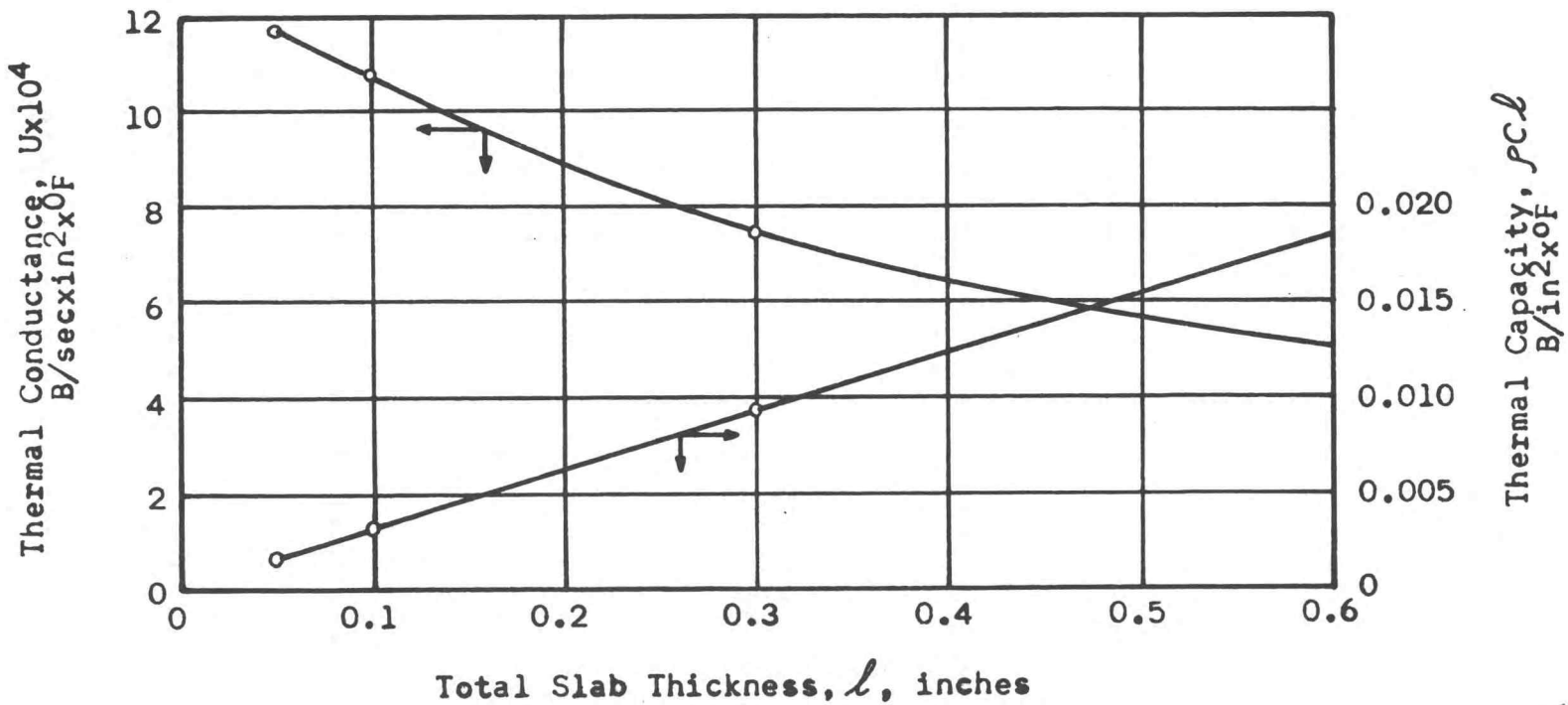

Figure 12. AN ILLUSTRATION OF THE DEVIATION OF THE APPROXIMATE METHOD FROM THE MATHEMATICAL METHOD OF ANALYSIS OF A SMALL SLAB SUBJECTED TO SUDDEN HEATING AND COOLING

Mathematical method ——————

Approximate method — — — — — —

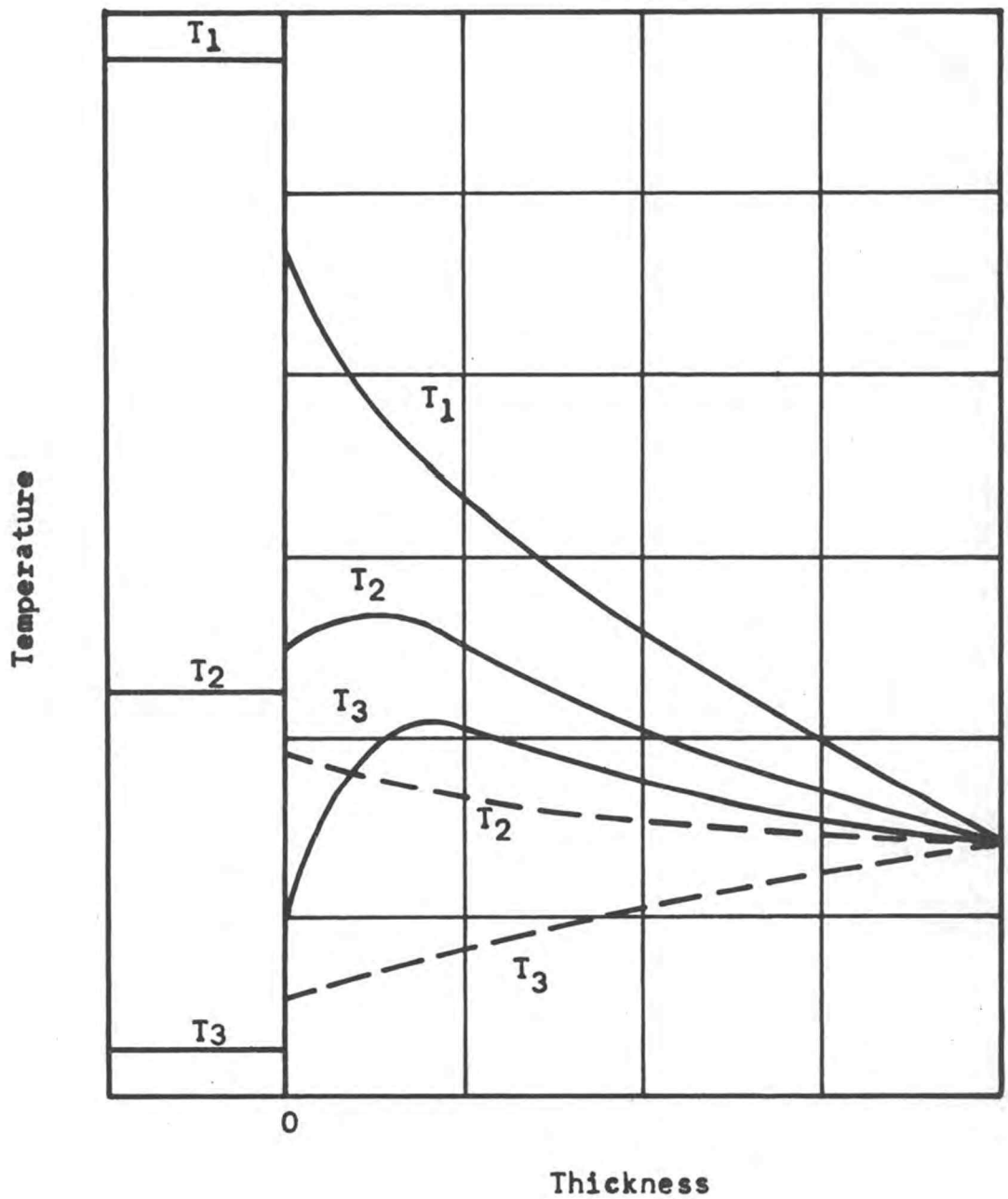

Figure 13. TEMPERATURE VARIATION OF THE RELAXATION TIME OF POLYCRYSTALLINE Al_2O_3

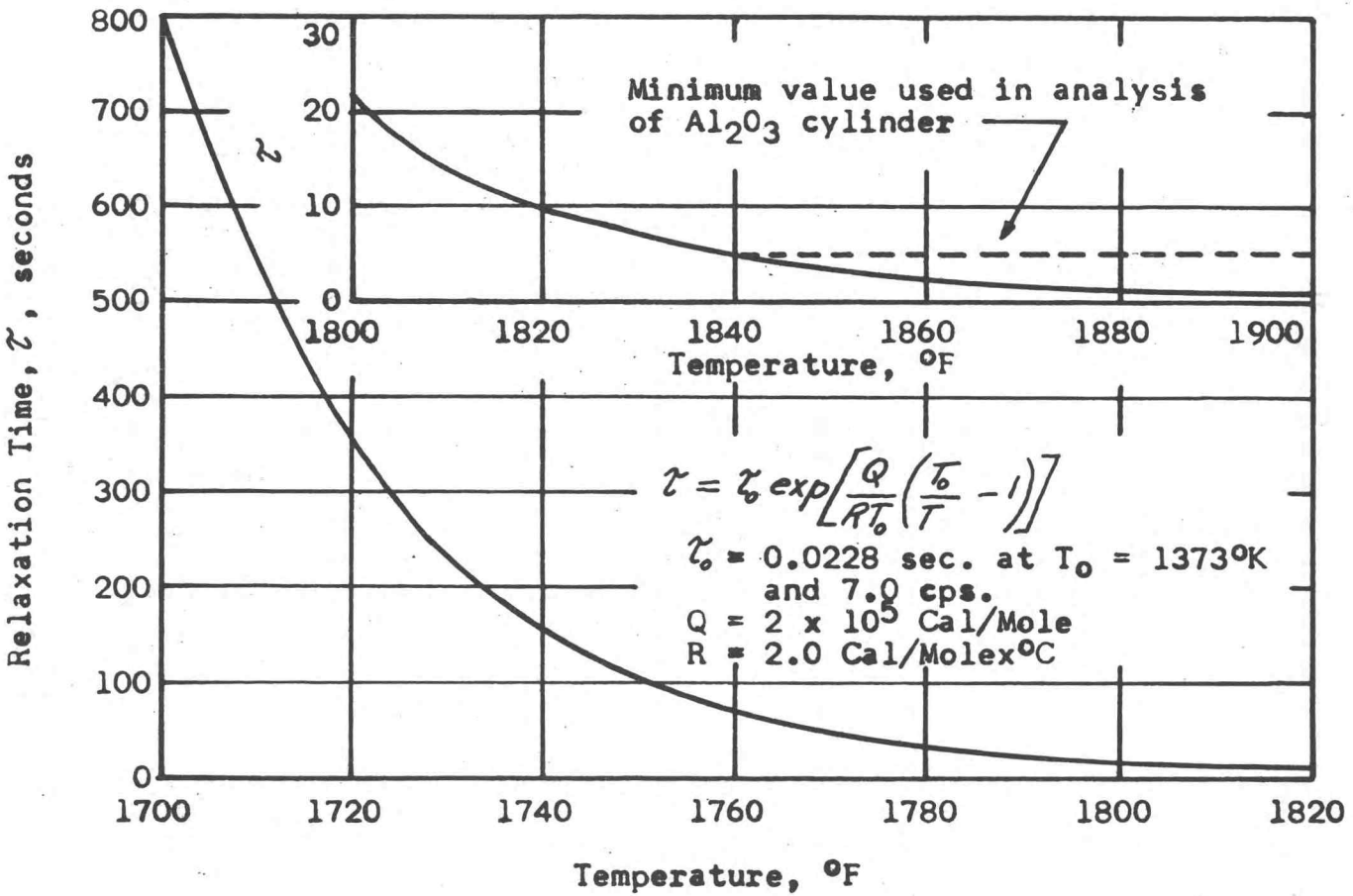

Figure 14. AN INFINITE MATRIX OF SQUARE COOLING CHANNELS IN A HEAT GENERATING MEDIUM

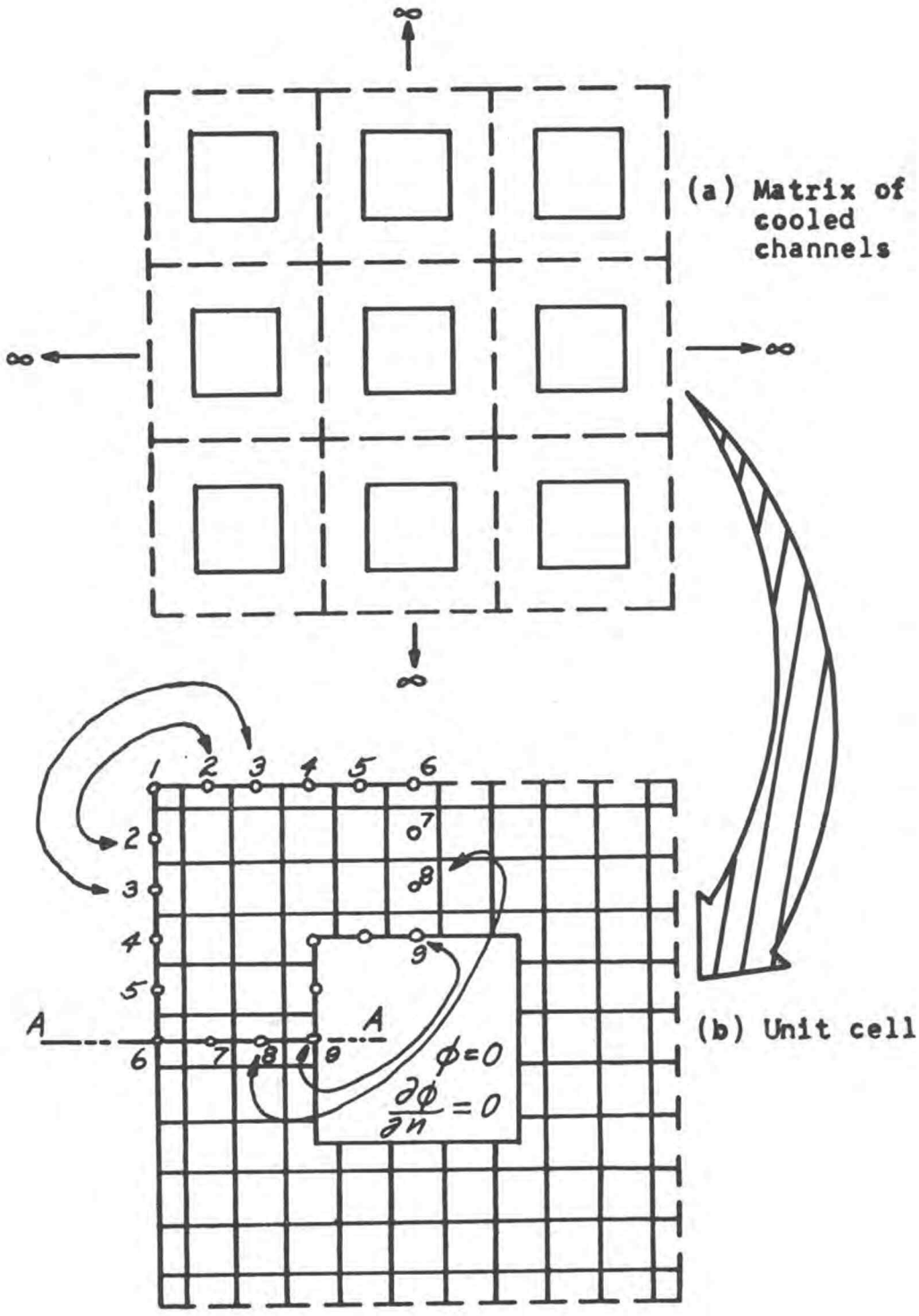

Figure 15. A MAP OF THE STRESS FUNCTION IN A UNIT CELL IN AN INFINITE MATRIX OF CELLS

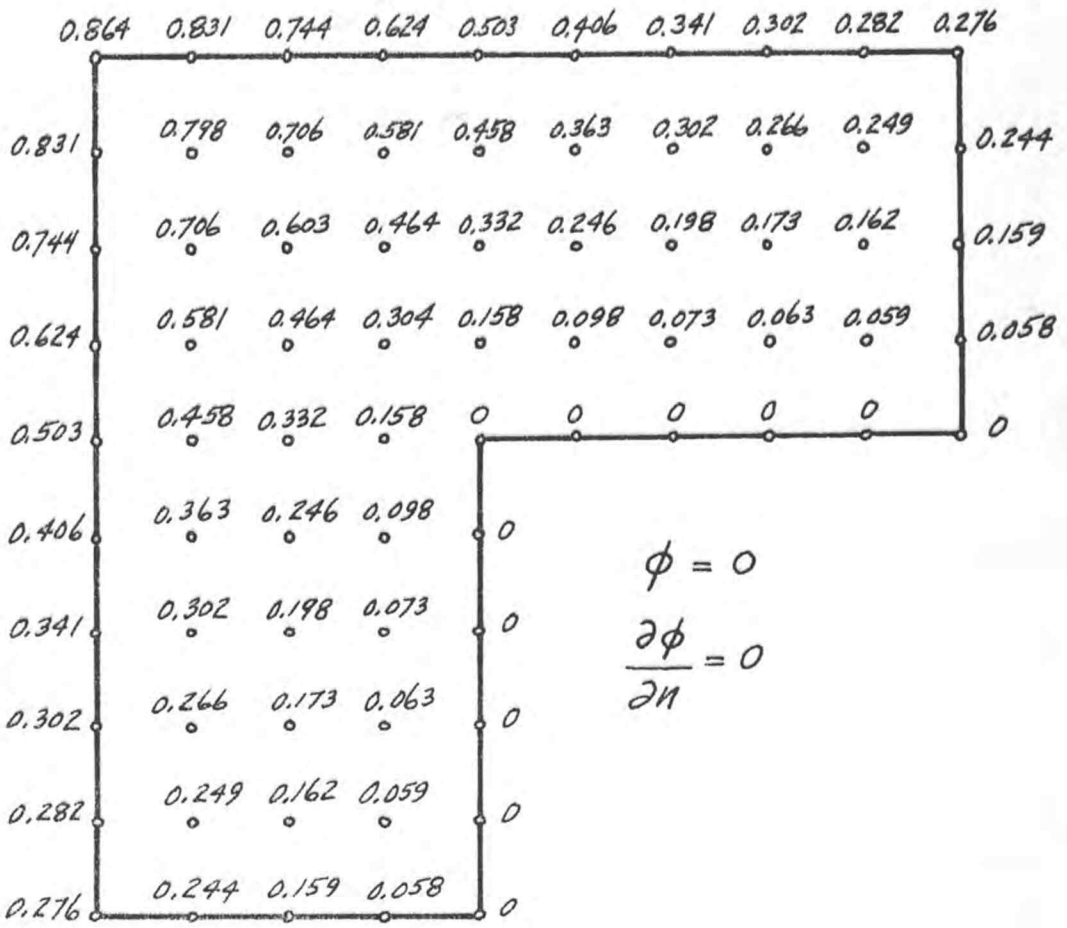

Figure 16. A MAP OF THE STRESSES IN A UNIT CELL IN AN INFINITE MATRIX OF CELLS

Legend:

Stresses in x-direction: 21

Stresses in y-direction: (413)

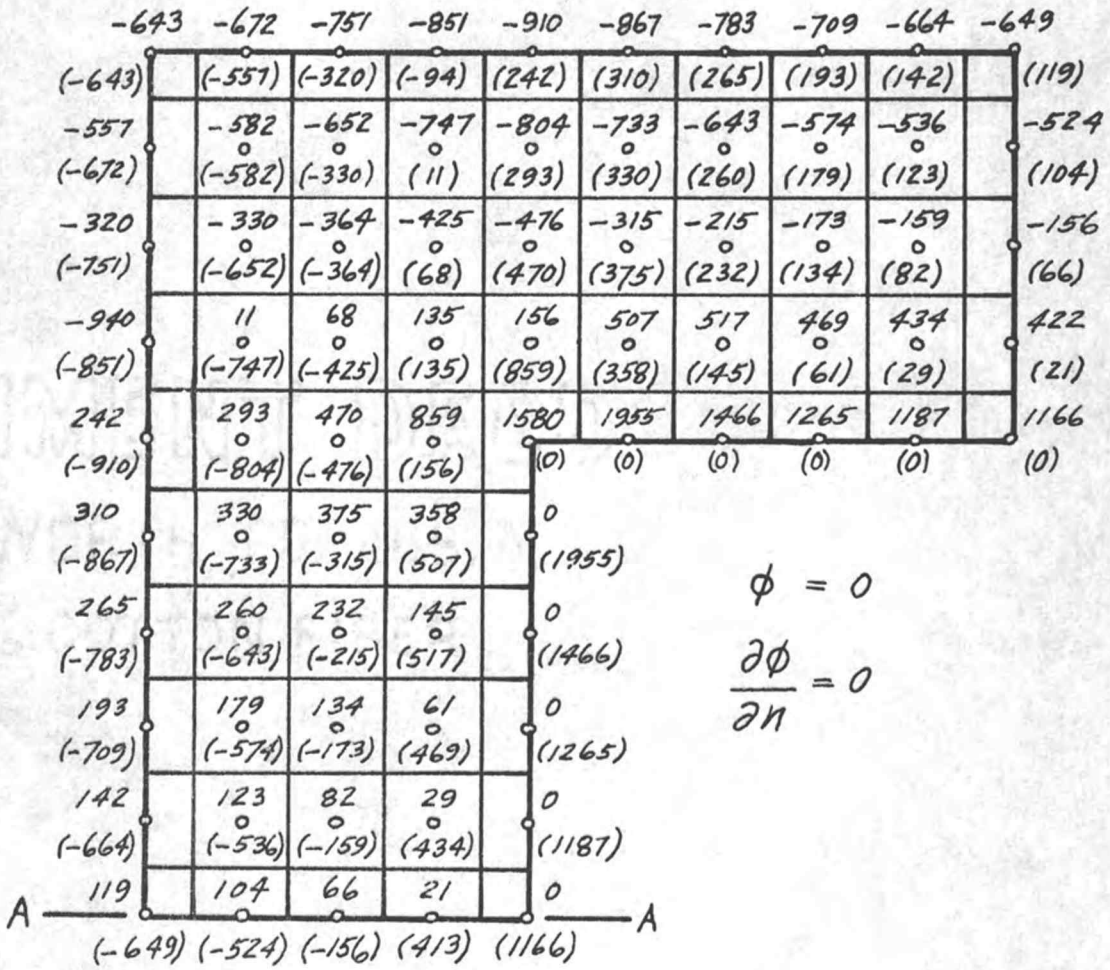

Figure 17. THERMAL STRESS DISTRIBUTION IN THE WALL OF A SQUARE UNIT CELL IN AN INFINITE MATRIX OF CELLS

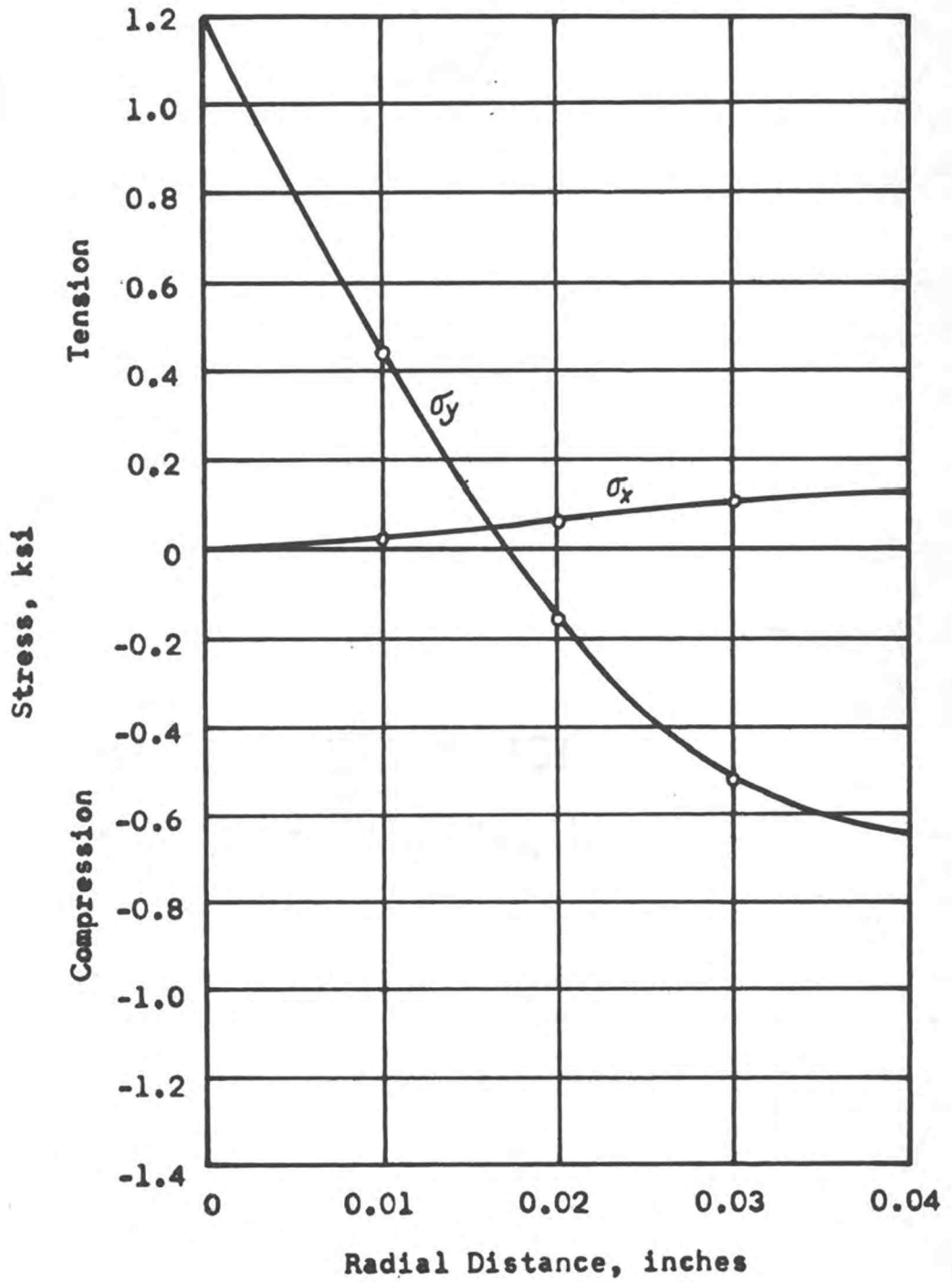

Figure 18. HEAT GENERATION AND CALCULATED TEMPERATURES IN A UNIT CELL

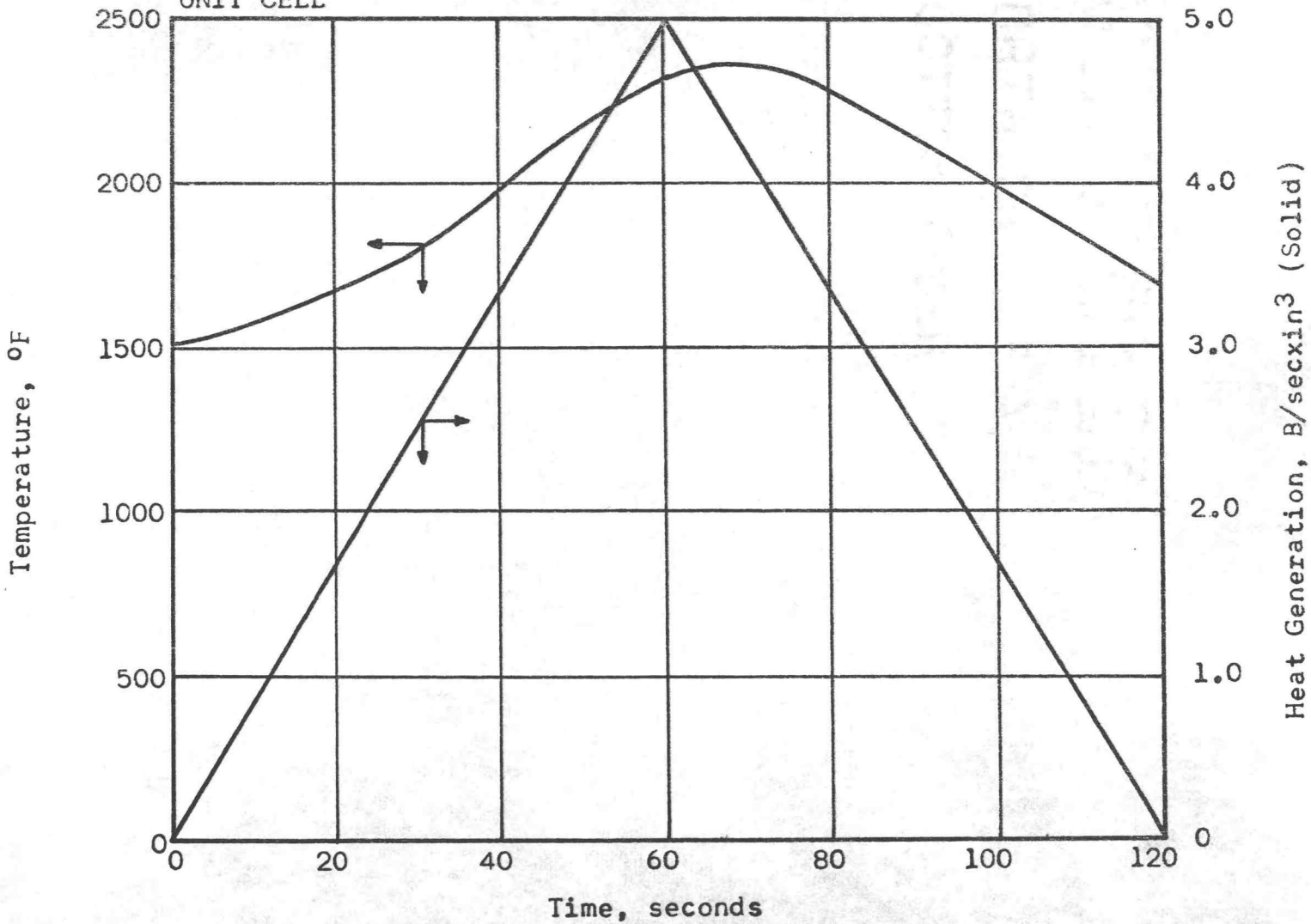

Figure 19. CALCULATED MAXIMUM TANGENTIAL THERMAL STRESSES IN A UNIT CELL

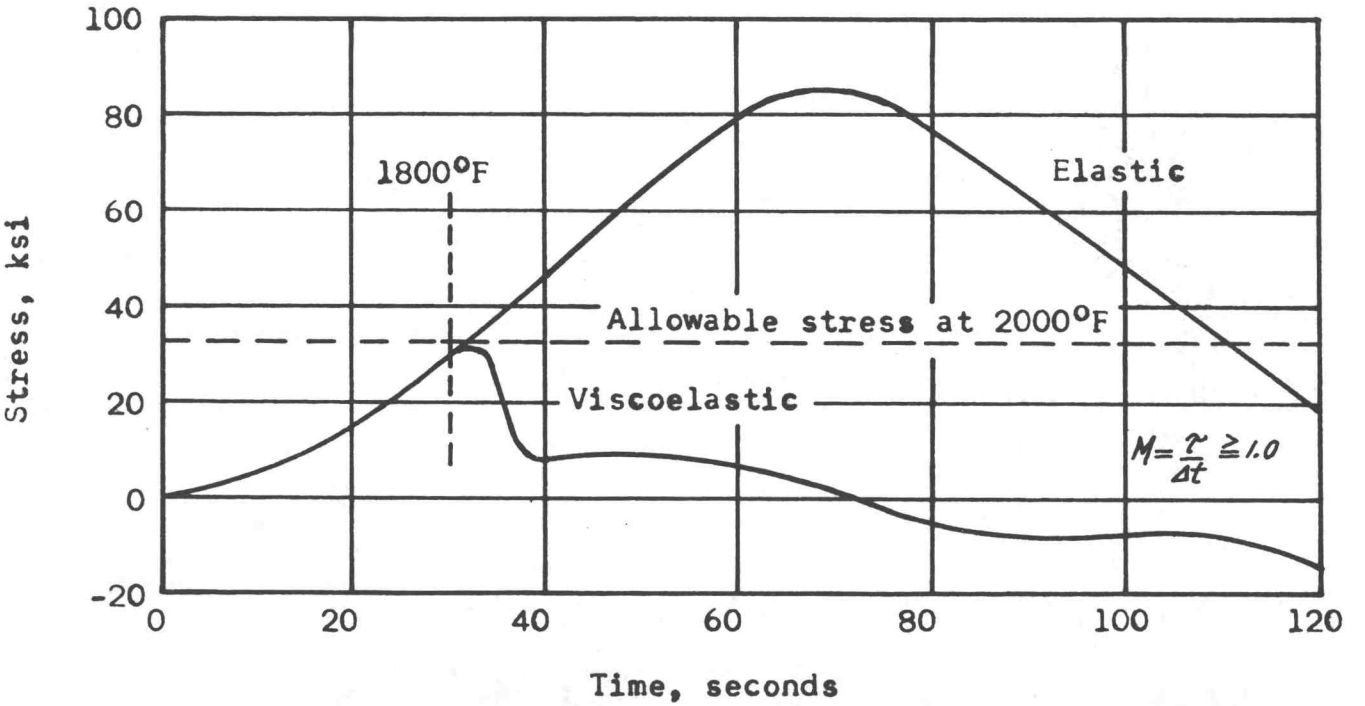

Figure 20. CALCULATED TANGENTIAL THERMAL STRESSES IN THE PERFORATED CYLINDER

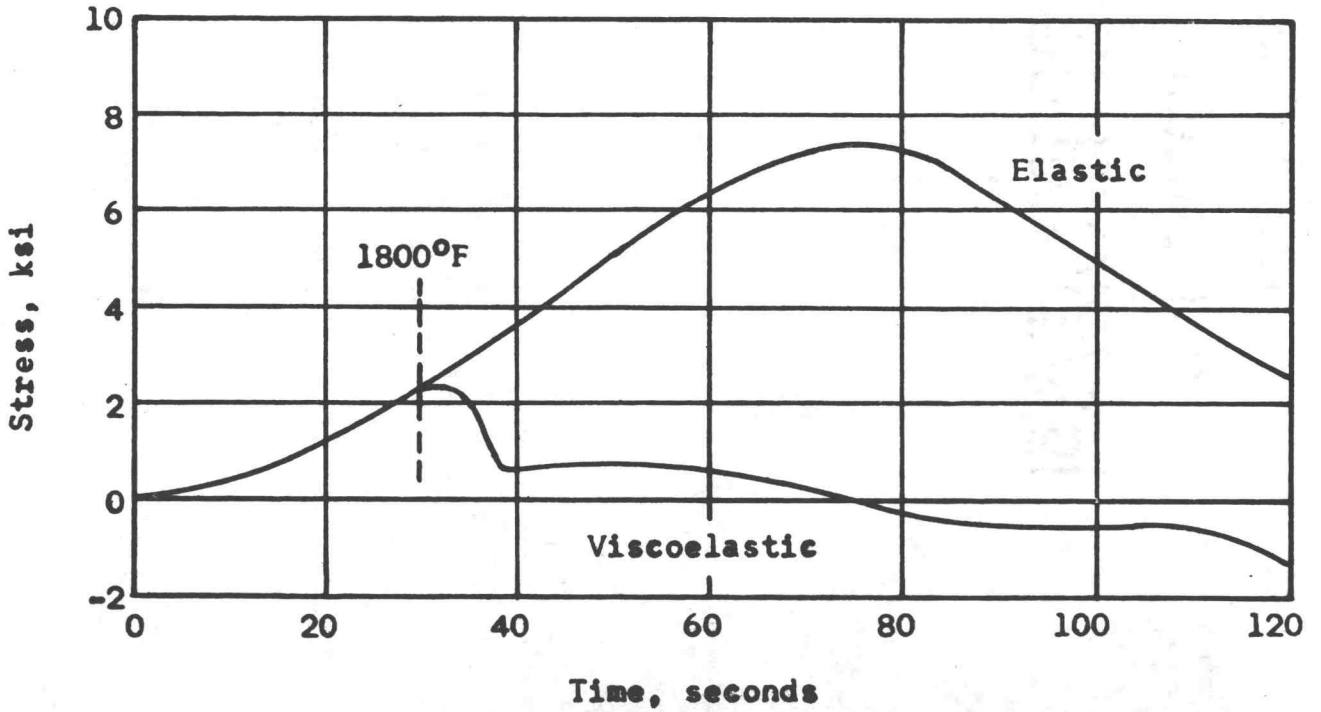

Figure 21. COMBINED CYLINDER AND UNIT CELL VISCOELASTIC TANGENTIAL THERMAL STRESSES

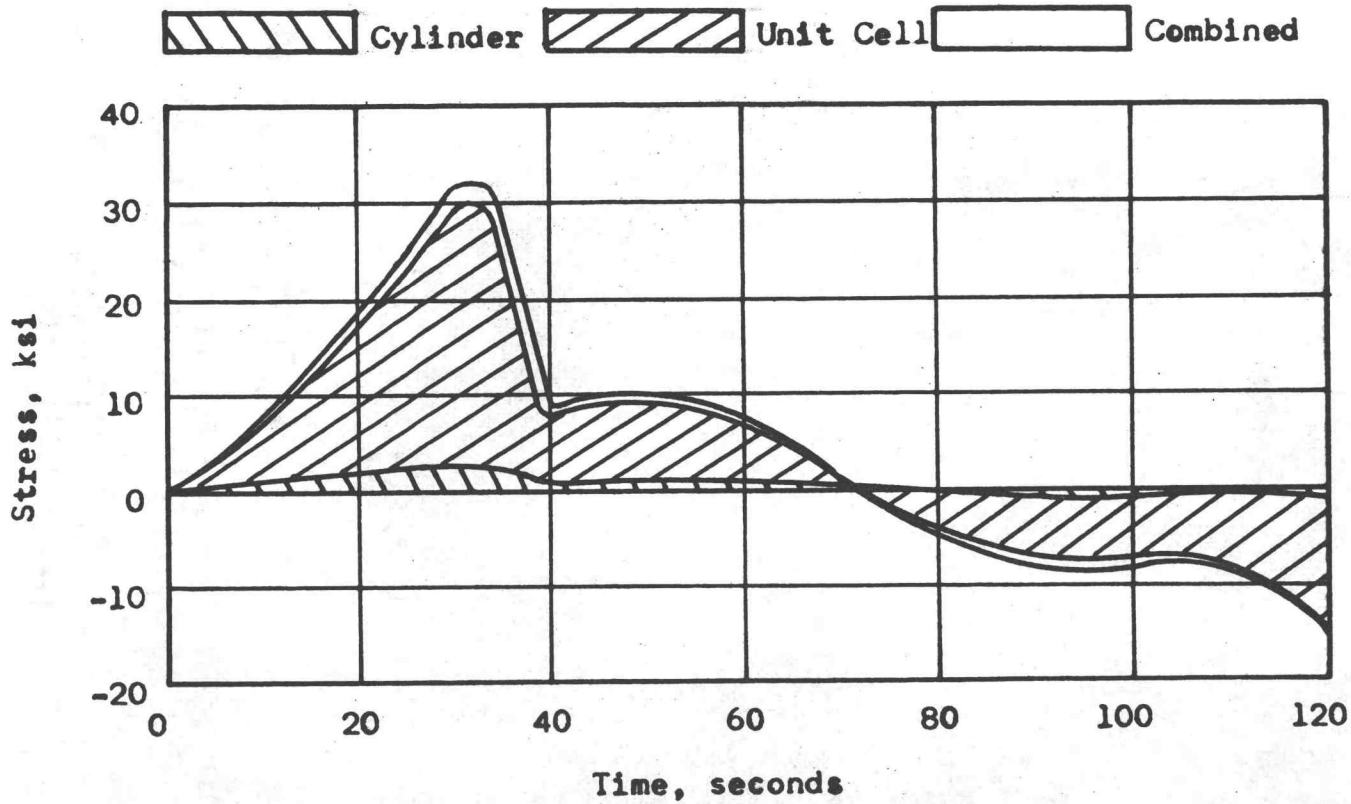

1. Bonilla, C. F. Nuclear engineering. New York, McGraw-Hill, 1957. 850 p.
2. Chang, Roger. Creep and anelastic studies of Al_2O_3. Canoga Park, Atomics International, 1958. 24 p. (North American Aviation, Inc. Report NAA-SR-2770)
3. Chang, Roger. Section Leader, Research Division, Atomics International. Canoga Park, December 1959.
4. Freudenthal, A. M. The inelastic behavior of engineering materials and structures. New York, John Wiley and Sons, 1950. 587 p.
5. Horvay, G. Stresses in perforated sheets due to non-uniform heating. Schenectady, Knolls Atomic Power Laboratory, 1951. 39 p. (Knolls Atomic Power Laboratory Report KAPL-566)
6. Horvay, G. The plane-stress problem of perforated plates. Journal of Applied Mechanics 19:355-360. 1952.
7. Jakob, Max. Heat transfer. Vol. 1. New York, John Wiley and Sons, 1949. 758 p.
8. Timoshenko, S. and J. N. Goodier. Theory of elasticity. New York, McGraw-Hill, 1951. 506 p.

APPENDICES

DETERMINATION OF THE INSTABILITY OF THE FINITE DIFFERENCE EQUATIONS FOR HEAT CONDUCTION IN A UNIT CELL

The finite difference representation of the differential system (Equation 1) which defines the heat transfer process in a unit cell is expressed by the following equations:

Interior Points

$$T_{m,n+1} = \left\{ \frac{(r_m + r_{m+1})}{2r_m} T_{m+1,n} + \frac{(r_{m-1} + r_m)}{2r_m} T_{m-1,n} + \left[\frac{\rho_{m,n} C_{m,n} \Delta r^2}{k_{o,m,n} \Delta t} - \frac{(r_{m+1} - 2r_m + r_{m-1})}{2r_m} \right] T_{m,n} \right\} \div \left(\frac{\rho_{m,n} C_{m,n} \Delta r^2}{k_{o,m,n} \Delta t} \right) \quad (A\text{-}1)$$

Convection Boundary Point

$$T_{m,n+1} = \left\{ \frac{(r_m + r_{m+1}) T_{m+1,n}}{r_m} + \frac{2 h_{m,n} \Delta r T_o}{k_{o,m,n}} + \left[\frac{\rho_{m,n} C_{m,n} \Delta r^2}{k_{o,m,n} \Delta t} - \frac{(r_m + r_{m+1})}{r_m} - \frac{2 h_{m,n} \Delta r}{k_{o,m,n}} \right] T_{m,n} \right\} \div \left(\frac{\rho_{m,n} C_{m,n} \Delta r^2}{k_{o,m,n} \Delta t} \right). \quad (A\text{-}2)$$

The stability of Equation (A-1) is determined by the coefficient of $T_{m,n}$. Rewriting Equation (A-1)

$$T_{m,n+1} = \frac{A T_{m+1,n} + B T_{m-1,n} + C T_{m,n}}{M} \qquad (A\text{-}1)$$

$$= F_1 T_{m+1,n} + F_2 T_{m-1,n} + F_3 T_{m,n} \qquad (A\text{-}1)$$

where

$$F_1 = \frac{A}{M} \qquad (A\text{-}3)$$

$$F_2 = \frac{B}{M} \qquad (A\text{-}4)$$

$$F_3 = \frac{C}{M} = \frac{M-A-B}{M} . \qquad (A\text{-}5)$$

The requirement is that $F_3 \geqq 0$ otherwise Equation (A-1) will become unstable and values of T_m will oscillate. When $F_3 \geqq 0$

then

$$\frac{\rho_{m,n} C_{m,n} \Delta r^2}{k_{o,m,n} \Delta t} = M \geqq A + B = \frac{r_{m+1} + 2r_m + r_{m-1}}{2r_m}$$

$$= \frac{r_m + \Delta r + 2r_m + r_m - \Delta r}{2r_m}$$

$$= \frac{4r_m}{2r_m} = 2.$$

Therefore, the requirement for stability of Equation (A-1) is:

$$M = \frac{\rho_{m,n} C_{m,n} \Delta r^2}{k_{o,m,n} \Delta t} \geqq 2 \qquad (A\text{-}6)$$

The stability of Equation (A-2) is determined in a similar manner. The requirement for Equation (A-2) is:

$$M = \frac{\rho_{m,n} C_{m,n} \Delta r^2}{k_{o,m,n} \Delta t} \geqq 2 + \frac{\Delta r}{r_m} + \frac{2 k_{m,n} \Delta r}{k_{o,m,n}} . \qquad (A\text{-}7)$$

A plot of M for the equivalent cylinder model of the aluminum oxide unit cell of Figure 2, as a function of time of operation, is presented as Figure 4. The temperatures at which the thermal properties were evaluated are presented as Figure 5. The base lines labeled "boundary" and "interior" on Figure 4 represent the values of M below which the respective equations would be unstable.

DERIVATION OF AN APPROXIMATE METHOD OF DETERMINING THE TRANSIENT TEMPERATURE DISTRIBUTIONS IN A UNIT CELL AND A COMPARISON WITH A MATHEMATICAL SOLUTION

Consider the equivalent cylinder model of a unit cell shown in Figure B1.

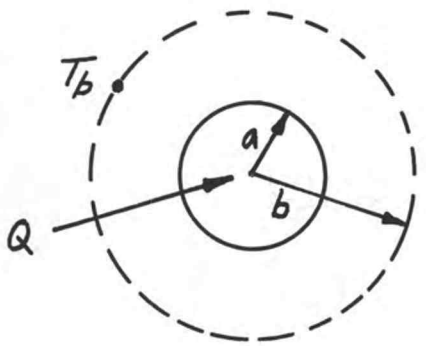

Figure B1

Ideally, in order to find the temperature distributions in this cylinder under transient conditions and with internal heat generation the following differential system would be solved:

$$k_0 \nabla^2 T + q_{v0} = \rho c \frac{\partial T}{\partial t} \qquad (B\text{-}1)$$

(1) $T = T_i$ at $t = 0$, $r = r$

(2) $\frac{\partial T}{\partial r} = 0$ at $r = b$, $t = t$

(3) $k_0 \frac{\partial T}{\partial r} = h(T - T_0)$ at $r = a$, $t = t$.

It is virtually impossible to solve this system when k_o, q_{vo}, ρ, C and h vary drastically with time and/or temperature. For the equivalent cylinder model of the unit cell of Figure 2 the finite difference approximation of this system has already been ruled out as impractical (see Appendix A).

An approximate method of determining the transient temperature distributions in the unit cell model has been devised. The approximate method has been used on a simple slab geometry and the results compared with those of the mathematical solution to establish confidence in the method and to determine under what conditions the method fails. Three cases have been selected to illustrate variations of the approximate method. The first case deals with an isolated unit cell in which the heat generated in the unit cell is the only heat flowing to the cooling passage. The second case deals with a unit cell which is one of many in a perforated geometry. In the second case, the temperature distribution in the perforated geometry has been determined by considering conduction through the geometry, heat generation in the unit cells and heat lost from the unit cells (this case is treated analytically in Appendix C). In this second case then, the unit cell heat generation has been used and the unit cell maximum temperature calculated. The information to be obtained from the

second case would be the temperature distribution in the unit cell for thermal stress or other purposes. The third case considered is that of a simple isolated slab without heat generation, heated only by gas flowing over one surface. The results of this case are used to show the deviation of the results of the approximate method from those of the mathematical solution.

Case 1: Isolated Unit Cell with Heat Generation

The unit cell model on page 50 is treated as one region and the heat balance is

$$\pi(b^2-a^2)\rho C \frac{dT_b}{dt} = \pi(b^2-a^2)q_{vo} - 2\pi a U(T_b-T_o) \qquad (B-2)$$

or

$$\frac{dT_b}{dt} = \frac{q_{vo}}{\rho C} - \frac{2aU(T_b-T_o)}{(b^2-a^2)\rho C}. \qquad (B-3)$$

Equation (B-3) may be used for a transient situation, where q_{vo}, ρ, C and U are varying, by applying to each increment of time Δt. This is done by considering all the variable quantities constant over the small time interval and that the unit cell temperature at the beginning of each time interval, $T_{b,n}$ is the final temperature, $T_{b,n+1}$ computed for the previous time interval. Each time interval begins at a time zero and ends at a time Δt.

The solution of Equation (B-3) for a time interval is

$$\frac{A - B(T_{b,n+1} - T_o)}{A - B(T_{b,n} - T_o)} = \exp(-B\Delta t) \qquad (B\text{-}4)$$

where

$$A = \frac{q_{vo}}{\rho C}$$

$$B = \frac{2aU}{(b^2 - a^2)\rho C}.$$

During the transient operation defined by Equation (B-2), the heat flowing through the unit cell wall is

$$Q = 2\pi a U (T_b - T_o).$$

In the one region model considered, this heat flow will produce a steady-state temperature distribution since the storage and generation of heat occurs at the outer boundary only. In the actual case, both heat storage and generation will be distributed in some manner over the unit cell radius and will not produce the same temperature distribution as the usual steady-state. A reasonable approximation of the correct temperature distribution must be made for the calculation of thermal stress. The simplest approximation one can make in lieu of more detailed study would be to consider the heat flowing through the unit cell wall as heat generated in the wall and distribute it uniformly as a volumetric heat generation. For this

approximation, the temperature distribution in the unit cell model is defined by the following differential system:

$$\frac{d^2T}{dr^2} + \frac{1}{r}\frac{dT}{dr} + \frac{q'_{vo}}{k_o} = 0 \qquad (B\text{-}5)$$

$$(1)\ \frac{dT}{dr} = 0 \quad at\ r = b$$

$$(2)\ k_o \frac{dT}{dr} = h(T - T_o) \quad at\ r = a$$

where

$$q'_{vo} = \frac{2\pi a U (T_b - T_o)}{\pi (b^2 - a^2)}. \qquad (B\text{-}6)$$

The solution of system (B-5) is

$$T = \frac{q'_{vo}}{4k_o}(a^2 - r^2) + \frac{q'_{vo}}{2k_o}\ln\frac{r}{a} + \frac{q'_{vo}(b^2 - a^2)}{2ah} + T_o. \qquad (B\text{-}7)$$

The overall heat transfer coefficient, U, must be compatible with the system (B-5) and Equation (B-6). Substituting Equation (B-7), evaluated at $r = b$, into Equation (B-6) and rearranging, we get

$$U = \frac{\pi q'_{vo}(b^2 - a^2)}{2\pi a\left[\frac{q'_{vo}}{4k_o}(a^2 - b^2) + \frac{q'_{vo}b^2}{2k_o}\ln\frac{b}{a} + \frac{q'_{vo}}{2ah}(b^2 - a^2) + T_o - T_o\right]}$$

or

$$U = \frac{(b^2 - a^2)}{\frac{a(a^2 - b^2)}{2k_o} + \frac{ab^2}{k_o}\ln\frac{b}{a} + \frac{(b^2 - a^2)}{h}}. \qquad (B\text{-}8)$$

An alternate solution may be obtained using Equation (B-6) if the unit cell wall temperature, T_w, at $r=a$, is known. For this alternate solution

$$q'_{vo} = \frac{2\pi a h (T_w - T_o)}{\pi (b^2 - a^2)} . \qquad (B-9)$$

Case 2: A Unit Cell Which is One of Many in a Cooled Perforated Geometry with Internal Heat Generation

In this case, the maximum temperature in the unit cell is the same as that calculated for the perforated geometry at that location (see Appendix C). In this case it is necessary only to find the temperature distribution in the unit cell wall using Equations (B-6), (B-7) and (B-8).

Case 3: Isolated Slab without Heat Generation, Heated Only by Gas Flowing Over One Surface

The main purpose for considering the case of this slab is to show how the approximate method deviates from the mathematical solution. The mathematical solution for the slab geometry is simpler than that for a cylinder. The semi-infinite slab used in this case is shown in Figure B2.

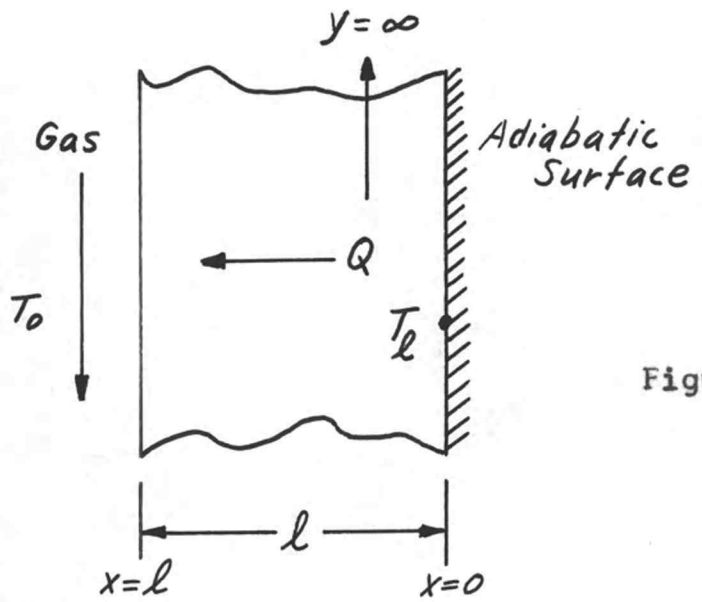

Figure B2

1. Approximate method

The slab is treated as one region the same as the unit cell in Case 1. The heat balance on the slab is

$$\rho C A \ell \frac{dT_\ell}{dt} = -UA(T_\ell - T_0) \qquad (B\text{-}10)$$

or

$$\frac{dT_\ell}{dt} = \frac{-U}{\rho C \ell}(T_\ell - T_0). \qquad (B\text{-}11)$$

The solution to Equation (B-11) is

$$\frac{T_{\ell,n+1} - T_0}{T_{\ell,n} - T_0} = \exp\left(\frac{-U\Delta t}{\rho C \ell}\right). \qquad (B\text{-}12)$$

An approximation of the temperature distribution in the slab would be obtained in the same manner as in Case 1.

In this case the approximate temperature distribution is defined by the differential system

$$\frac{d^2T}{dx^2} + \frac{q'_{vo}}{k_o} = 0 \qquad (B\text{-}13)$$

$$(1)\ \frac{dT}{dx} = 0 \quad \text{at } x = 0$$

$$(2)\ -k_o \frac{dT}{dx} = h(T - T_o) \quad \text{at } x = l$$

where

$$q'_{vo} = \frac{UA(T_l - T_o)}{Al}. \qquad (B\text{-}14)$$

The solution of system (B-13) is

$$T = \frac{q'_{vo}}{2k_o}(l^2 - x^2) + \frac{q'_{vo}l}{h} + T_o. \qquad (B\text{-}15)$$

The overall heat transfer coefficient, U, must be compatible with the system (B-13) and Equation (B-14). Substituting Equation (B-15), evaluated at $x = 0$, into Equation (B-14) and rearranging we get

$$U = \frac{1}{\frac{l}{2k_o} + \frac{1}{h}}. \qquad (B\text{-}16)$$

If the surface temperature at $X=\ell$ is known, an alternate solution similar to that of Case 1 may be obtained by using

$$q'_{vo} = \frac{hA(T_w - T_o)}{A\ell} . \qquad (B\text{-}17)$$

2. Mathematical solution

The differential system which defines the transient heat transfer process in the slab is

$$\frac{\partial^2 T}{\partial x^2} = \frac{\rho c}{k_o}\frac{\partial T}{\partial t} \qquad (B\text{-}18)$$

(1) $\frac{\partial T}{\partial x} = 0$ at $x=0,\ t=t$

(2) $-k_o \frac{\partial T}{\partial x} = h(T-T_o)$ at $x=\ell,\ t=t$

(3) $T = T_i$ at $x=x,\ t=0.$

The solution to this system is

$$T = T_o + \sum_{n=1}^{\infty}\left[\frac{2(T_i-T_o)\sin\lambda_n \cos\left(\frac{\lambda_n x}{\ell}\right)}{\sin\lambda_n\cos\lambda_n + \lambda_n}\right]\exp\left(\frac{-\lambda_n^2 k_o t}{\rho c \ell^2}\right)$$

$$(n = 1, 2, 3 \ldots\ldots \text{etc}) \qquad (B\text{-}19)$$

where λ_n is defined by

$$\lambda_n \tan\lambda_n = \frac{h\ell}{k_o} . \qquad (B\text{-}20)$$

3. Comparison of the approximate method with the mathematical solution

The approximate method was compared to the mathematical solution by evaluation at four slab thicknesses. The temperatures at stations $x = 0$ and $x = \ell$ 3.0 seconds after the start of heating were compared and the percent deviation of the approximate method from the mathematical solution computed. The percent deviation as a function of slab thickness is presented in Figure 6. The computations are based upon the following conditions:

$T_o = 1000^o$ F

$T_i = 100^o$ F

$\rho = 0.137$ lbs/in^3

C = 0.23 B/lbs ^oF

$k_o = 2.48 \times 10^{-4}$ B/sec x in x ^oF

$h = 1.33 \times 10^{-3}$ B/sec x in^2 x ^oF.

The slab thicknesses considered were 0.05, 0.1, 0.3 and 0.6 inches. A summary of the results is presented in Table I.

The shape of the curve representing the interior point of a slab in Figure 6 can best be explained by considering the conductance and thermal capacity of the slab as shown in Figure 11. At large slab thicknesses the conductance u (see Equation B-11) is small and the thermal capacity $\rho c \ell$ is large. These conditions result in a

small heat influx and a small heat storage which give a large ΔT in the slab and a small temperature rise. At small slab thicknesses u is large and $\rho c l$ is small. This results in a large heat influx and a large heat storage which give a small ΔT and a large temperature rise.

By simpler reasoning, it becomes obvious that as the total slab thickness increases the percent deviation of the temperature of the interior point, calculated by the approximate method, from that calculated by the mathematical method would become smaller. At sufficiently large slab thicknesses and small times the temperature of the interior point calculated by both methods would approach the initial temperature. At larger slab thicknesses, however, as shown by Figure 6, the error in the surface temperature would continue to increase. The error in the surface temperature, however, would decrease at greater times.

The approximate method cannot evaluate sudden heating or cooling such as in quenching, etc. A typical example of such a situation is shown in Figure 12. The approximate method can only operate with the source temperature, conductance and thermal capacitance of the slab. The temperature distributions which might be obtained by the approximate method are shown by dotted lines in Figure 12.

HEAT TRANSFER IN PERFORATED GEOMETRIES WITH VOLUMETRIC HEAT DISSIPATION AND VOLUMETRIC HEAT GENERATION

The differential equation which describes the heat transfer process in an object with multiple heat sinks and with internal heat generation is

$$k\nabla^2 T - U_v(T-T_0) + q_v = \rho C \frac{\partial T}{\partial t} \qquad (C\text{-}1)$$

where

$k\nabla^2 T$ = the conduction term

$U_v(T-T_0)$ = the term for dissipation due to multiple sinks

q_v = the internal heat generation term

$\rho C \frac{\partial T}{\partial t}$ = the storage term.

The solution of Equation (C-1) is not difficult to obtain for common shapes such as cylinders, slabs, etc. However, most practical problems require numerical methods of solution since k, U_v, q_v, ρ and C vary with temperature or time.

The quantities k, q_v and ρ are "apparent" values based upon the total volume of the object and are functions of the true values for the solid material and the void fraction in the object. The apparent thermal

conductivity, k , is defined as

$$k = k_0 \left(\frac{1-B}{1+\frac{B}{3}} \right) \qquad \text{(7, p. 85)} \qquad (C\text{-}2)$$

where

k_0 = the solid material thermal conductivity

and

B = the void fraction.

Jakob (7, p. 85) mentions that similar forms of this equation may be valid up to $B = 0.5$.

The apparent volumetric heat generation, q_V , is defined as

$$q_V = q_{oV} (1-B) \qquad (C\text{-}3)$$

where

q_{oV} = the volumetric heat generation for the solid material.

The apparent density, ρ , is defined as

$$\rho = \rho_o (1-B) \qquad (C\text{-}4)$$

where

ρ_o = the density of the solid material.

The volumetric heat dissipation coefficient, U_V , is derived from a consideration of the heat transfer in a

unit cell. For a differential length of cooling passage, the heat transferred in a unit cell (see Appendix B) is

$$Q = 2\pi a U (T-T_0) dx. \qquad (C-5)$$

If we base this heat flow on the total volume of the unit cell we can write

$$2\pi a U (T-T_0) dx = \pi b^2 U_V (T-T_0) dx \qquad (C-6)$$

or

$$U_V = \frac{2aU}{b^2}. \qquad (C-7)$$

Now the void fraction for the unit cell is

$$B = \frac{\pi a^2 dx}{\pi b^2 dx} = \frac{a^2}{b^2} \qquad (C-8)$$

therefore Equation (C-7) becomes

$$U_V = \frac{2uB}{a}. \qquad (C-9)$$

It is clearly evident, then, that the analysis of the heat transfer process in an object with multiple heat sinks and with internal heat generation involves the treatment of "lumped" heat sinks as "distributed" heat sinks in Equations (C-1) and (C-6). In a numerical method of analysis, where the object is divided into discrete regions, a "re-lumping" of the distributed heat sinks is necessary.

APPENDIX D

DERIVATION OF THE THERMAL STRESS EQUATIONS FOR A MAXWELL CYLINDER BASED ON THE ELASTIC VISCOELASTIC ANALOGY

The simplest idealization of the mechanical response of materials at elevated temperatures that includes both the elastic and the creep component of the deformation is the linear viscoelastic response (1, p. 578-595). The linear viscoelastic response combines the linear elastic (Hookean) relation between stress and strain with the linear viscous (Newtonian) relation between stress and strain rate to produce a material that responds nearly elastically to rapidly applied loads but creeps under loads of longer duration (Maxwell body) (4, p. 205).

The Maxwell body may be represented by a spring and dashpot model as shown in Figure D1.

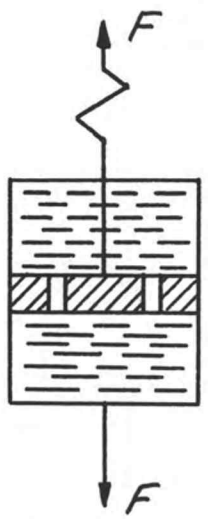

Figure D1

For a cylinder under conditions of plane strain the combination of the equilibrium equations

$$\frac{\partial \sigma_r}{\partial r} + \frac{1}{r}(\sigma_r - \sigma_\theta) = 0 \qquad (D\text{-}1)$$

$$\frac{\partial \sigma_z}{\partial z} = 0 \qquad (D\text{-}2)$$

and the compatibility condition

$$\frac{\partial \epsilon_\theta}{\partial r} + \frac{1}{r}(\epsilon_\theta - \epsilon_r) = 0 \qquad (D\text{-}3)$$

with the linear viscoelastic stress-strain relations,

$$2G\left[\frac{\partial \epsilon_r}{\partial t} - \frac{1}{3}\left(\frac{\partial \epsilon_r}{\partial t} + \frac{\partial \epsilon_\theta}{\partial t} + \frac{\partial \epsilon_z}{\partial t}\right)\right] = \left(\frac{\partial}{\partial t} + \frac{1}{\tau}\right)\left[\sigma_r - \frac{1}{3}(\sigma_r + \sigma_\theta + \sigma_z)\right] \qquad (D\text{-}4)$$

$$2G\left[\frac{\partial \epsilon_\theta}{\partial t} - \frac{1}{3}\left(\frac{\partial \epsilon_r}{\partial t} + \frac{\partial \epsilon_\theta}{\partial t} + \frac{\partial \epsilon_z}{\partial t}\right)\right] = \left(\frac{\partial}{\partial t} + \frac{1}{\tau}\right)\left[\sigma_\theta - \frac{1}{3}(\sigma_r + \sigma_\theta + \sigma_z)\right] \qquad (D\text{-}5)$$

$$2G\left[\frac{\partial \epsilon_z}{\partial t} - \frac{1}{3}\left(\frac{\partial \epsilon_r}{\partial t} + \frac{\partial \epsilon_\theta}{\partial t} + \frac{\partial \epsilon_z}{\partial t}\right)\right] = \left(\frac{\partial}{\partial t} + \frac{1}{\tau}\right)\left[\sigma_z - \frac{1}{3}(\sigma_r + \sigma_\theta + \sigma_z)\right] \qquad (D\text{-}6)$$

the compressibility equation,

$$K\left(\frac{\partial \epsilon_r}{\partial t} + \frac{\partial \epsilon_\theta}{\partial t} + \frac{\partial \epsilon_z}{\partial t}\right) = 3\left[\frac{(\sigma_r + \sigma_\theta + \sigma_z)}{3} + K\alpha\frac{\partial T}{\partial t}\right] \qquad (D\text{-}7)$$

and the plane strain condition

$$\frac{\partial \epsilon_z}{\partial t} = 0 \qquad (D\text{-}8)$$

produces two simultaneous partial differential equations for σ_r and σ_θ that can be separated only by the assumption of imcompressibility ($K \to \infty, \mu = 0.5$). In this case, the equation for σ_r for the Maxwell cylinder can be directly written on the basis of the elastic viscoelastic analogy in the following manner:

Assuming incompressibility, and the plane strain condition, Equation (D-7) reduces to

$$\frac{\partial \epsilon_r}{\partial t} + \frac{\partial \epsilon_\theta}{\partial t} = 3\alpha \frac{\partial T}{\partial t}. \qquad (D\text{-}9)$$

Solving Equation (D-6) for σ_z we get

$$\left(\frac{\partial}{\partial t} + \frac{1}{\tau}\right)\sigma_z = -3G\alpha \frac{\partial T}{\partial t} + \left(\frac{\partial}{\partial t} + \frac{1}{\tau}\right)(\sigma_r + \sigma_\theta). \qquad (D\text{-}10)$$

Substituting from Equation (D-10) into Equations (D-4) and (D-5) and solving for $\frac{\partial \epsilon_r}{\partial t}$ and $\frac{\partial \epsilon_\theta}{\partial t}$.

$$\frac{\partial \epsilon_r}{\partial t} = \frac{3}{2}\alpha \frac{\partial T}{\partial t} + \frac{1}{4G}\left(\frac{\partial}{\partial t} + \frac{1}{\tau}\right)(\sigma_r - \sigma_\theta) \qquad (D\text{-}11)$$

$$\frac{\partial \epsilon_\theta}{\partial t} = \frac{3}{2}\alpha \frac{\partial T}{\partial t} + \frac{1}{4G}\left(\frac{\partial}{\partial t} + \frac{1}{\tau}\right)(\sigma_\theta - \sigma_r). \qquad (D\text{-}12)$$

Rewriting Equation (D-3) as

$$\frac{\partial \epsilon_r}{\partial t} = r\frac{\partial^2 \epsilon_\theta}{\partial r \partial t} + \frac{\partial \epsilon_\theta}{\partial t} \qquad (D\text{-}13)$$

and substituting from Equations (D-11) and (D-12) we obtain

$$\left(\frac{\partial}{\partial t}+\frac{1}{\tau}\right)(\sigma_r-\sigma_\theta)=\frac{3}{2}r\alpha\frac{\partial^2 T}{\partial r\partial t}+\frac{r}{4G}\left(\frac{\partial}{\partial t}+\frac{1}{\tau}\right)\frac{\partial}{\partial r}(\sigma_\theta-\sigma_r). \quad (D\text{-}14)$$

Finally, using the equilibrium Equation (D-1), we get a differential equation for the radial stress

$$\left(\frac{\partial}{\partial t}+\frac{1}{\tau}\right)\frac{\partial}{\partial r}\left(r^3\frac{\partial\sigma_r}{\partial r}\right)=-6Gr^2\alpha\frac{\partial^2 T}{\partial r\partial t}. \quad (D\text{-}15)$$

Integrating Equation (D-15) with respect to r and dividing by r^3 gives

$$\left(\frac{\partial}{\partial t}+\frac{1}{\tau}\right)\left(\frac{\partial\sigma_r}{\partial r}\right)=-\frac{6G\alpha}{r}\frac{\partial T}{\partial t}+\frac{12G\alpha}{r^3}\int_a^r r\frac{\partial T}{\partial t}dr+\frac{C_1}{r^3}. \quad (D\text{-}16)$$

Integrating again with respect to r reduces Equation (D-16) to

$$\left(\frac{\partial}{\partial t}+\frac{1}{\tau}\right)\sigma_r=-\frac{6G\alpha}{r^2}\int_a^r r\frac{\partial T}{\partial t}dr-\frac{C_1}{2}\left(\frac{a^2-r^2}{a^2r^2}\right)+C_2 \quad (D\text{-}17)$$

where C_1 and C_2 are constants of integration.
Substituting Equations (D-16) and (D-17) into Equation (D-1) we obtain the tangential stress equation

$$\left(\frac{\partial}{\partial t}+\frac{1}{\tau}\right)\sigma_\theta=\frac{6G\alpha}{r^2}\int_a^r r\frac{\partial T}{\partial t}dr-6G\alpha\frac{\partial T}{\partial t}+\frac{C_1}{2}\left(\frac{a^2+r^2}{a^2r^2}\right)+C_2$$

$$(D\text{-}18)$$

where

$$G = \frac{E}{2(1+\mu)} \qquad (D\text{-}19)$$

and

$$\tau = \frac{\eta}{G} . \qquad (D\text{-}20)$$

THE BOUNDARY CONDITIONS FOR THERMAL STRESS IN A UNIT CELL IN A PERFORATED GEOMETRY

1. Thermal Stresses in an Equivalent Cylinder Model of a Unit Cell with Conditions of Symmetry at the Outer Boundary

Consider a cluster of unit cells sufficiently large and operating under conditions such that a unit cell located in a particular region is exactly like those surrounding it. Under these conditions, the radial stress at the outer boundary of the equivalent cylinder model of the unit cell would equal that of each surrounding unit cell. No discontinuities are envisioned in the radial stresses at the outer boundaries and there are no applied forces inside the holes, therefore, the differential system which describes the steady-state elastic radial stress distribution in the unit cell is

$$\frac{d}{dr}\left(r^3 \frac{d\sigma_r}{dr}\right) = \beta r^2 \frac{dT}{dr} \qquad (E\text{-}1)$$

$$(1)\ \frac{d\sigma_r}{dr} = 0 \qquad \text{at} \quad r = b$$

$$(2)\ \sigma_r = 0 \qquad \text{at} \quad r = a$$

where $\beta = -\frac{\alpha E}{1-\mu}$.

The solution of this differential system is

$$\sigma_r = \frac{\beta}{r^2}\left\{\int_a^r Tr\,dr + \frac{(r^2-a^2)}{2a^2}\left[-b^2T(b) + 2\int_a^b Tr\,dr\right]\right\}. \quad (E\text{-}2)$$

Solution (E-2) yields a non-zero summation of moments across the radius of the unit cell model. To explain why this occurs and to justify the occurrence, the following analysis is presented.

Consider a unit cell in which the elastic thermal stresses are defined by the differential system

$$\left(\frac{d^2}{dr^2} + \frac{1}{r}\frac{d}{dr}\right)\left(\frac{d^2\phi_1}{dr^2} + \frac{1}{r}\frac{d\phi_1}{dr}\right) = \frac{\beta}{r}\frac{d}{dr}\left(r\frac{dT}{dr}\right) \quad (E\text{-}3)$$

(1) $\frac{d\sigma_r}{dr} = 0 \quad$ at $\quad r = b$

(2) $\sigma_r = 0 \quad$ at $\quad r = a$

(3) $\int_a^b \sigma_\theta r\,dr = 0$

where

$$\sigma_{r_1} = \frac{1}{r}\frac{d\phi_1}{dr}$$

and

$$\sigma_{\theta_1} = \frac{d^2\phi_1}{dr^2}.$$

The stresses obtained from the solution of the biharmonic equation are

$$\sigma_{r_1} = \frac{\beta}{r^2}\int_a^r Tr\,dr + \frac{A_1}{r^2} + B_1 + 2B_1 \ln r + 2C_1 \qquad (E\text{-}4)$$

and

$$\sigma_{\theta_1} = \beta T - \frac{\beta}{r^2}\int_a^r Tr\,dr - \frac{A_1}{r^2} + 3B_1 + 2B_1 \ln r + 2C_1 \qquad (E\text{-}5)$$

where A_1, B_1 and C_1 are constants of integration.

A complete solution to the system (E-3) is not possible without a consderation of the displacements. The radial displacement (u) and the tangential displacement (v) are defined by the equations:

$$\epsilon_r = \frac{\partial u}{\partial r} \qquad (E\text{-}6)$$

$$\epsilon_\theta = \frac{u}{r} + \frac{1}{r}\frac{\partial v}{\partial \theta} \qquad (E\text{-}7)$$

and

$$\gamma_{r\theta} = \frac{1}{r}\frac{\partial u}{\partial \theta} + \frac{\partial v}{\partial r} - \frac{v}{r}. \qquad (E\text{-}8)$$

From Hooke's Law (for plane strain)

$$\epsilon_r = \frac{1}{E}\left[\sigma_r - \mu(\sigma_\theta + \sigma_z) + E\alpha T\right] = \frac{\partial u}{\partial r} \qquad (E\text{-}9)$$

$$\epsilon_\theta = \frac{1}{E}\left[\sigma_\theta - \mu(\sigma_z + \sigma_r) + E\alpha T\right] = \frac{u}{r} + \frac{1}{r}\frac{\partial v}{\partial \theta} \qquad (E\text{-}10)$$

$$\epsilon_z = \frac{1}{E}\left[\sigma_z - \mu(\sigma_r + \sigma_\theta) + E\alpha T\right] = \text{Constant.} \qquad (E\text{-}11)$$

Solving Equation (E-11) for σ_z and substituting into (E-9) and (E-10) along with σ_r and σ_θ of (E-4) and (E-5) we obtain after integration

$$u = \frac{1}{E}\left[(1-\mu^2)\int \sigma_r\, dr - \mu(1+\mu)\int \sigma_\theta\, dr + (1+\mu)E\alpha \int T\, dr - \mu E \epsilon_z r\right] + f(\theta). \qquad (E\text{-}12)$$

From (E-10) we then obtain

$$\frac{\partial v}{\partial \theta} = r\epsilon_\theta - u = \frac{4}{E} B_1 r (1-\mu^2) - f(\theta). \qquad (E\text{-}13)$$

Integration of (E-13) gives

$$v = \frac{4}{E} B_1 r\theta (1-\mu^2) - \int f(\theta)\, d\theta + f(r). \qquad (E\text{-}14)$$

When Equations (E-12) and (E-14) are combined with Equation (E-8) when $\gamma_{r\theta}$ is zero and the resultant equation

integrated we obtain

$$f(r) = Fr \qquad (E\text{-}15)$$

and

$$f(\theta) = H\sin\theta + K\cos\theta. \qquad (E\text{-}16)$$

Therefore Equation (E-14) becomes

$$v = \frac{4}{E}(1-\mu^2)B_1 r\theta + Fr + H\cos\theta - K\sin\theta \qquad (E\text{-}17)$$

where F, H and K are constants of integration.

The first term in Equation (E-17) causes the tangential displacement v to become many-valued which is physically impossible in a full ring. For this reason the constant B_1 in the general solution of the system (E-3) is usually set equal to zero (8, p. 66-68). The purpose of the development of the analysis of which the complete solution of the differential system (E-3) is a part is to explain why a positive moment is obtained with the solution (E-2) and to justify its occurrence. For this reason, B_1 is not set equal to zero since the solution would revert back to that of (E-2) and the cause of the positive

moment would remain a mystery. When the boundary conditions

$$\left.\begin{aligned} u &= 0 \\ v &= 0 \\ \frac{\partial v}{\partial r} &= 0 \end{aligned}\right\} \quad \text{at } \theta = 0 \text{ and } r = \frac{a+b}{2} \qquad (E\text{-}18)$$

are imposed upon (E-17) we obtain

$$v = \frac{4}{E}(1-\mu^2)B_1 r\theta - K\sin\theta. \qquad (E\text{-}19)$$

At $\theta = 2\pi$, a tangential displacement

$$v = \frac{8\pi}{E}(1-\mu^2)B_1 r = \alpha r \qquad (E\text{-}20)$$

is the result of the conditions of system (E-3). To visualize this displacement assume that the system (E-3) applies to a hollow cylinder with a radial cut.

In order to restore the cylinder to its original condition, a mechanical force must be applied such that a displacement of opposite sign occurs, i.e.,

$$v = -\alpha r. \qquad (E\text{-}21)$$

The stresses in the cylinder due to the applied force are superimposed upon those of Equations (E-4) and (E-5) to obtain the stresses which would occur in the cylinder <u>if</u>

it had not been allowed to deflect. The mechanical stresses are defined by the differential system

$$\left(\frac{d^2}{dr^2}+\frac{1}{r}\frac{d}{dr}\right)\left(\frac{d^2\phi_2}{dr^2}+\frac{1}{r}\frac{d\phi_2}{dr}\right)=0 \qquad (E\text{-}22)$$

(1) $\frac{d\sigma_r}{dr}=0$ at $r=b$

(2) $\sigma_r=0$ at $r=a$.

The stresses obtained from the solution to this biharmonic equation are

$$\sigma_{r_2}=\frac{A_2}{r^2}+B_2+2B_2\ln r+2C_2 \qquad (E\text{-}23)$$

$$\sigma_{\theta_2}=\frac{-A_2}{r^2}+3B_2+2B_2\ln r+2C_2 \qquad (E\text{-}24)$$

where A_2, B_2 and C_2 are constants of integration.

The tangential displacement at $\theta=2\pi$ would be

$$v=\frac{8\pi}{E}(1-\mu^2)B_2 r. \qquad (E\text{-}25)$$

However, this displacement must be of opposite sign to that of (E-20), therefore

$$B_2=-B_1. \qquad (E\text{-}26)$$

Equations (E-23) and (E-24 are rewritten to give

$$\sigma_{r_2} = \frac{A_2}{r^2} - B_1 - 2B_1 \ln r + 2C_2 \qquad (E\text{-}27)$$

and

$$\sigma_{\theta_2} = \frac{-A_2}{r^2} - 3B_1 - 2B_1 \ln r + 2C_2 . \qquad (E\text{-}28)$$

From the boundary conditions of the systems (E-3) and (E-22) the constants of integration are

$$A_1 = -\left\{-2a^2b^2\left[\beta\int_a^b Tr\,dr - \beta\int_a^b \frac{1}{r}\left(\int_a^r Tr\,dr\right)dr\right] + a^2(2b^2\ln\frac{b}{a} + b^2 - a^2)\left[\frac{\beta b^2}{2}T(b) - \beta\int_a^b Tr\,dr\right]\right\} \div (b^2-a^2)^2 \qquad (E\text{-}29)$$

$$B_1 = -\left\{(2a^2\ln\frac{b}{a} + b^2 - a^2)\left[\frac{\beta b^2}{2}T(b) - \beta\int_a^b Tr\,dr\right] - 2a^2\left[\beta\int_a^b Tr\,dr - \beta\int_a^b \frac{1}{r}\left(\int_a^r Tr\,dr\right)dr\right]\right\} \div (b^2-a^2)^2 \qquad (E\text{-}30)$$

$$C_1 = -\left\{-\left[b^2\ln b + b^2 - a^2\ln a - a^2 + a^2(1+2\ln a)(\ln\frac{b}{a})\right]\right.$$
$$\times\left[\beta\frac{b^2}{2}T(b) - \beta\int_a^b Tr\,dr\right] + \left[a^2(1+2\ln a) + b^2\right]$$
$$\left.\times\left[\beta\int_a^b Tr\,dr - \beta\int_a^b \frac{1}{r}\left(\int_a^r Tr\,dr\right)dr\right]\right\}$$
$$\div (b^2-a^2)^2 \qquad (E\text{-}31)$$

$$A_2 = -B_1 b^2 \qquad (E\text{-}32)$$

and

$$C_2 = \frac{B_1}{2}\left(\frac{b^2}{a^2} + 1 + 2\ln a\right). \qquad (E\text{-}33)$$

When these constants are substituted in (E-4) and (E-23) and the equations added to produce $\sigma_{r_1} + \sigma_{r_2}$ we find that the resultant equation is identical to Equation (E-2). The moment

$$M = \int_a^b \sigma_{\theta_2} r\,dr \qquad (E\text{-}34)$$

is the same as that obtained from the solution of the system (E-1) and represents the moment exerted upon the unit cell by its surroundings to produce a zero radial stress gradient at the outer boundary of the unit cell and single-valued tangential displacements.

2. Thermal Stresses in a Unit Cell in a Square Matrix of Square Cooling Channels

Consider the infinite matrix of square cooling channels in a heat generating material as shown in Figure 14 (a). A unit cell is shown in Figure 14 (b).

In terms of the stress function, the thermal stresses in the unit cell may be expressed as

$$\frac{\partial^4\phi}{\partial x^4} + 2\frac{\partial^4\phi}{\partial x^2\partial y^2} + \frac{\partial^4\phi}{\partial y^4} = \frac{-\alpha E}{1-\mu}\left(\frac{\partial^2 T}{\partial x^2} + \frac{\partial^2 T}{\partial y^2}\right) = \frac{-\alpha E q_{vo}}{(1-\mu)k_o}. \qquad (E-35)$$

The boundary conditions at the cooling channel surfaces are defined by

$$\ell\frac{\partial^2\phi}{\partial y^2} - m\frac{\partial^2\phi}{\partial x\partial y} = \bar{X} = 0 \qquad (E-36)$$

and

$$m\frac{\partial^2\phi}{\partial x^2} - \ell\frac{\partial^2\phi}{\partial x\partial y} = \bar{Y} = 0 \qquad (E-37)$$

where $\bar{X}$ and $\bar{Y}$ are the forces acting in the x and y directions, respectively, and ℓ and m are the direction cosines of normals to the boundary. In the x direction

$$\bar{X} = \bar{Y} = 0 \qquad \text{(no normal forces)}$$
$$m = 0$$

and $\ell = 1$.

Similarly for the y direction

$$\bar{x} = \bar{y} = 0$$

$$\ell = 0$$

and $m = 1.$

Substitution of these terms in Equations (E-36) and (E-37) and integration yields the boundary conditions

$$\frac{\partial \phi}{\partial n} = \frac{\partial \phi}{\partial x} = \frac{\partial \phi}{\partial y} = \phi \quad (n = \text{normal to surface}).$$

A finite difference approximation of the differential system represented by Equations (E-35) and (E-38) creates a system of equations for the stress function at the various nodes in Figure 14 (b). The simulation of an infinite matrix of unit cells may be accomplished by connecting like numbered nodes as shown in Figure 14 (b).

At conditions nearly approximating those in the equivalent cylinder model of the unit cell of Figure 2, an analysis was made to determine the thermal stress distributions in the square unit cell of Figure 14 (b). The conditions used are:

$$q_{v0} = 1.7 \text{ B/sec x in}^3$$

$$k_0 = 2.48 \times 10^{-4} \text{ B/sec x in x } ^\circ\text{F}$$

$$\mu = 0.3$$

$$\alpha E = 236 \text{ lb/in}^2 \text{ x } ^\circ\text{F}$$

Web thickness = 0.04 inch

Node spacing = 0.01 inch

The solution of the system of equations with these conditions produced a map of the stress function as shown in Figure 15. The definition of the stress function states that

$$\sigma_x = \frac{\partial^2 \phi}{\partial y^2}$$

$$\sigma_y = \frac{\partial^2 \phi}{\partial x^2}$$

$$\tau_{xy} = -\frac{\partial^2 \phi}{\partial x \partial y}.$$

Using these definitions, the stress map of Figure 16 was constructed. The stresses along the radial line A-A in Figure 16 are plotted in Figure 17. The curves in Figure 17 indicate that the slope of the curve for σ_x (σ_x corresponds to the radial stresses, σ_r, in a cylindrical unit cell model) is zero at the outer boundary. The curve for the stress σ_y (σ_y corresponds to the tangential stress, σ_θ, in a cylindrical unit cell) is of the same shape and magnitude one would expect of a curve of σ_θ for the cylindrical unit cell with the conditions $\sigma_r = 0$ not $\frac{d\sigma_r}{dr} = 0$ at the outer boundary.

It is recommended that for the computation of the tangential stresses in a cylindrical model of the unit

cell the condition at the outer boundary be specified as $\sigma_r = 0$ rather than $\frac{d\sigma_r}{dr} = 0$.

SOLUTION OF THE INELASTIC THERMAL STRESS EQUATIONS FOR THE UNIT CELL AND CYLINDER BY NUMERICAL METHODS AND THE DETERMINATION OF THE STABILITY REQUIREMENTS

Most studies of practical importance which require the determination of the viscoelastic stresses usually involve time and temperature variable material properties, ambient conditions, etc. In such cases the solution of the viscoelastic equations must be obtained by numerical methods and this in turn requires the additional consideration of equation stability.

1. Unit Cell

The equations for inelastic thermal stresses based upon the elastic viscoelastic analogy for a cylinder are

$$\left(\frac{\partial}{\partial t}+\frac{1}{\tau}\right)\frac{\partial}{\partial r}\left(r^3\frac{\partial \sigma_r}{\partial r}\right)=-6Gr^2\alpha\frac{\partial^2 T}{\partial r\,\partial t} \qquad (F\text{-}1)$$

(See Appendix D, Equation D-15)

and

$$\left(\frac{\partial}{\partial t}+\frac{1}{\tau}\right)\sigma_\theta=\left(\frac{\partial}{\partial t}+\frac{1}{\tau}\right)\left(\sigma_r+r\frac{\partial \sigma_r}{\partial r}\right). \qquad (F\text{-}2)$$

Consider the term $\frac{\partial^2 T}{\partial r\,\partial t}$ in Equation (F-1). This may be approximated for an increment of time by

$$\frac{\partial^2 T}{\partial r\,\partial t}=\frac{d}{dr}\left(\frac{T_{n+1}-T_n}{t_{n+1}-t_n}\right). \qquad (F\text{-}3)$$

At any instant of time, if we assume that the heat dissipation or absorption may be distributed volumetrically as discussed in Appendix B, we can approximately represent the heat flow in the unit cell as a steady state process. Only q_v and k will change with time. Therefore

$$T_{n+1} = \frac{-q_{v,n+1} r^2}{4k_{n+1}} + A \ln r + B \qquad (F\text{-}4)$$

and

$$T_n = \frac{-q_{v,n} r^2}{4k_n} + C \ln r + D \qquad (F\text{-}5)$$

where A, B, C, and D are constants of integration.

The boundary conditions at any instant of time, if we define T as the excess of temperature above the wall temperature (temperature at inner radius), would be

$$\left.\begin{aligned} &(1)\ \frac{dT}{dr} = 0 \quad \text{at} \quad r = b \\ &(2)\ T = 0 \quad \text{at} \quad r = a. \end{aligned}\right\} \qquad (F\text{-}6)$$

Imposing the conditions (F-6) on Equations (F-4) and (F-5) we obtain

$$T_{n+1} = \frac{q_{v,n+1}}{k_{n+1}}\left[\frac{(a^2 - r^2)}{4} + \frac{b^2}{2}\ln\frac{r}{a}\right] \qquad (F\text{-}7)$$

and

$$T_n = \frac{q_{v,n}}{k_n}\left[\frac{(a^2 - r^2)}{4} + \frac{b^2}{2}\ln\frac{r}{a}\right]. \qquad (F\text{-}8)$$

The time derivative of the temperature is then approximately represented by

$$\frac{\partial T}{\partial t} \cong \left(\frac{\frac{q_{v,n+1}}{k_{n+1}} - \frac{q_{v,n}}{k_n}}{t_{n+1} - t_n} \right) \left[\frac{(a^2 - r^2)}{4} + \frac{b^2}{2} \ln \frac{r}{a} \right] \qquad (F\text{-}9)$$

and Equation (F-3) may be written

$$\frac{\partial^2 T}{\partial r \partial t} \cong \left(\frac{\frac{q_{v,n+1}}{k_{n+1}} - \frac{q_{v,n}}{k_n}}{t_{n+1} - t_n} \right) \left(\frac{-r}{2} + \frac{b^2}{2r} \right) = \xi_\varphi \left(\frac{-r}{2} + \frac{b^2}{2r} \right). \qquad (F\text{-}10)$$

Substituting from (F-10) into (F-1) and integrating with respect to r we obtain

$$\left(\frac{\partial}{\partial t} + \frac{1}{\tau} \right) \sigma_r = -3G\alpha \xi_\varphi \left(\frac{b^2}{2} \ln r - \frac{r^2}{8} \right) - \frac{C_1}{2r^2} + C_2. \qquad (F\text{-}11)$$

When we impose the boundary conditions discussed in part B of Appendix E (conditions E-1), i.e.,

$$\left.\begin{array}{ll} (1) \quad \sigma_r = 0 & \text{at} \quad r = b \\ (2) \quad \sigma_r = 0 & \text{at} \quad r = a \end{array}\right\} \qquad (F\text{-}12)$$

we can write

$$\left(\frac{\partial}{\partial t} + \frac{1}{\tau} \right) \sigma_r = 3G\alpha \xi_\varphi \left[\frac{-(a^2 + b^2 - r^2)}{8} - \frac{b^2}{2} \ln \frac{r}{a} + \frac{a^2 b^2}{8r^2} - \left(\frac{1}{2r^2} - \frac{1}{2a^2} \right) \frac{a^2 b^4}{(b^2 - a^2)} \ln \frac{b}{a} \right] \qquad (F\text{-}13)$$

and from (F-2)

$$\left(\frac{\partial}{\partial t}+\frac{1}{\tau}\right)\sigma_\theta = 3G\alpha\xi_\varphi\left\{-\frac{a^2}{8}-\frac{5b^2}{8}+\frac{3r^2}{8}-\frac{b^2}{2}\ln\frac{r}{a}-\frac{a^2b^2}{8r^2}\right.$$
$$\left.-\left[\frac{1}{2}\left(\frac{a^2-r^2}{a^2r^2}\right)-\frac{1}{r^2}\right]\left[\frac{a^2b^4}{(b^2-a^2)}\ln\frac{b}{a}\right]\right\} \qquad (F\text{-}14)$$

$$= 3G\alpha\xi_\varphi\mathcal{F}_r. \qquad (F\text{-}15)$$

The maximum stress in the cylindrical model of the unit cell will be the tangential component at radius "a" and Equation (F-15) becomes

$$\left(\frac{\partial}{\partial t}+\frac{1}{\tau}\right)\sigma_\theta = 3G\alpha\xi_\varphi\left[\frac{a^2}{4}-\frac{3b^2}{4}+\frac{b^4}{(b^2-a^2)}\ln\frac{b}{a}\right] \qquad (F\text{-}16)$$

$$= 3G\alpha\xi_\varphi\mathcal{F}_a. \qquad (F\text{-}17)$$

The finite difference approximation of (F-17) is

$$\frac{\sigma_{\theta,n+1}-\sigma_{\theta,n}}{\Delta t} = -\frac{\sigma_{\theta,n}}{\tau_n}+3G\alpha\mathcal{F}_a\left(\frac{\frac{\varrho_{v,n+1}}{\rho_{n+1}}-\frac{\varrho_{v,n}}{\rho_n}}{\Delta t}\right). \qquad (F\text{-}18)$$

If we set

$$M = \frac{\tau_n}{\Delta t} \qquad (F\text{-}19)$$

and

$$N = 3G\alpha\mathcal{F}_a\tau_n\left(\frac{\frac{\varrho_{v,n+1}}{\rho_{n+1}}-\frac{\varrho_{v,n}}{\rho_n}}{\Delta t}\right) = 3G\alpha\mathcal{F}_a\tau_n\xi_\varphi \qquad (F\text{-}20)$$

then Equation (F-18) may be written

$$(\sigma_{\theta,n+1} - \sigma_{\theta,n}) = \frac{-\sigma_{\theta,n} + N}{M}$$

or

$$\sigma_{\theta,n+1} = \frac{(M-1)\sigma_{\theta,n} + N}{M}. \qquad (F-21)$$

Equation (F-21) is stable when

$$\frac{M-1}{M} \geqq 0$$

or

$$M = \frac{\tau_n}{\Delta t} \geqq 1. \qquad (F-22)$$

2. Perforated Parent Cylinder

For the perforated parent cylinder, Equation (F-1) is written as

$$\left(\frac{\partial}{\partial t} + \frac{1}{\tau}\right)\left(\frac{\partial^2 \sigma_R}{\partial R^2} + \frac{3}{R}\frac{\partial \sigma_R}{\partial R}\right) = -2E\alpha R^2 \frac{\partial^2 T}{\partial R \partial t} \qquad (F-23)$$

where R = the variable radius of the parent cylinder

$E = 2(1+\mu)G.$

A restriction on the use of the elastic viscoelastic analogy is that the material must be assumed to be incompressible (Poisson's ratio, $\mu = 0.5$), therefore $E = 3G$ (see Appendix D). The modulus of elasticity E in Equation (F-23)

is modified for perforated geometries as suggested by Horvay (6, p. 355-360).

The finite difference approximation to Equation (F-23) is developed in the following manner:

$$\left(\frac{\partial}{\partial t}+\frac{1}{\tau}\right)\left[\left(\frac{\sigma_{R,m+1}-2\sigma_{R,m}+\sigma_{R,m-1}}{H^2}\right)+\frac{3}{2HR_m}\left(\sigma_{R,m+1}-\sigma_{R,m-1}\right)\right]$$

$$=\frac{-2E_m\alpha_m}{R_m}\frac{\partial}{\partial t}\left(\frac{\Delta T}{\Delta R}\right)_m \qquad (F\text{-}24)$$

$$(m=0,1,2\ \cdots\ \text{etc})$$

where H = node spacing.

$$\text{Let}\quad \Sigma=\left(\frac{\sigma_{R,m+1}-2\sigma_{R,m}+\sigma_{R,m-1}}{H2}\right)+\frac{3}{2HR_m}\left(\sigma_{R,m+1}-\sigma_{R,m-1}\right) \qquad (F\text{-}25)$$

and

$$A_m=\frac{-2E_m\alpha_m}{R_m}. \qquad (F\text{-}26)$$

Therefore Equation (F-24) becomes

$$\left(\frac{\partial}{\partial t}+\frac{1}{\tau}\right)\Sigma=A_m\frac{\partial}{\partial t}\left(\frac{\Delta T}{\Delta R}\right)_m \qquad (F\text{-}27)$$

or in finite difference form

$$\frac{\Sigma_{n+1}-\Sigma_n}{\Delta t}+\frac{\Sigma_n}{\tau_n}=A_{m,n}\left[\frac{\Delta}{\Delta t}\left(\frac{\Delta T}{\Delta R}\right)_m\right]_n. \qquad (F\text{-}28)$$

Finally, substituting (F-25) and (F-26) into (F-28)

$$\left[\left(\frac{\sigma_{R,m+1}-2\sigma_{R,m}+\sigma_{R,m-1}}{H^2}\right)_{n+1}+\frac{3}{2HR_m}\left(\sigma_{R,m+1}-\sigma_{R,m-1}\right)_{n+1}\right.$$

$$\left.-\left(\frac{\sigma_{R,m+1}-2\sigma_{R,m}+\sigma_{R,m-1}}{H^2}\right)_{n}-\frac{3}{2HR_m}\left(\sigma_{R,m+1}-\sigma_{R,m-1}\right)\right]$$

$$\div \Delta t+\frac{1}{\tau_n}\left[\left(\frac{\sigma_{R,m+1}-2\sigma_{R,m}+\sigma_{R,m-1}}{H^2}\right)_{n}\right.$$

$$\left.+\frac{3}{2HR_m}\left(\sigma_{R,m+1}-\sigma_{R,m-1}\right)_{n}\right]$$

$$=-2\left(\frac{E\alpha}{R}\right)_{m,n}\left[\frac{\Delta}{\Delta t}\left(\frac{\Delta T}{\Delta R}\right)_m\right]_n. \qquad (F\text{-}29)$$

The initial values of stress for a time increment will be known, therefore the final values must be determined by solving the equations, for each radial position, simultaneously. The term $\frac{\Delta}{\Delta t}\left(\frac{\Delta T}{\Delta R}\right)$ is determined beforehand from the heat transfer methods described in Appendix C. If we set

$$M=\frac{\tau_n}{\Delta t} \qquad (F\text{-}30)$$

and

$$N=\frac{A_{m,n}}{\tau_n}\left[\frac{\Delta}{\Delta t}\left(\frac{\Delta T}{\Delta R}\right)_m\right]_n \qquad (F\text{-}31)$$

then Equation (F-28) may be written

$$\Sigma_{n+1} = \frac{N + (M-1)\Sigma_n}{M}. \qquad (F-32)$$

The stability requirement for this equation is

$$\frac{M-1}{M} \geqq 0. \qquad (F-33)$$

or

$$M = \frac{\tau_n}{\Delta t} \geqq 1. \qquad (F-34)$$

When the radial stresses in the perforated cylinder are determined from Equation (F-29), the tangential stresses are obtained by applying

$$\sigma_{\theta,m,n} = \sigma_{R,m,n} + R_m \left(\frac{\sigma_{R,m+1} - \sigma_{R,m-1}}{2H}\right)_n. \qquad (F-35)$$

The tangential stresses of Equation (F-35) are superimposed upon those of Equation (F-18), for the same location in the cylinder, to obtain an estimate of the maximum thermal stresses in the cylinder.

a = The inner radius of a unit cell

A = Heat transfer area

b = Outer radius of an equivalent cylinder model of a unit cell

B = Void fraction

C = Heat capacity

E = Modulus of elasticity

$\mathcal{F}$ = A geometric factor for computing the tangential thermal stress in an equivalent cylinder model of a unit cell

$\mathcal{F}_r$, at radius r.

$\mathcal{F}_a$, at radius a.

G = Modulus of rigidity

h = Heat transfer coefficient of convection

H = Radial node spacing for calculating thermal stresses in the perforated cylinder by finite differences

i = Denotes initial conditions

k = Thermal conductivity

k, of the perforated cylinder

k_o, of the unit cell or slab

K = Bulk modulus

l = Length of slab

m = Denotes a point in space

M = Moment

M = Stability factor

n = Denotes a point in time

q_v = Volumetric heat generation

q_v, in the perforated cylinder

q_{v_o}, in the unit cell

q'_{v_o}, a fictitious value for the unit cell or slab derived from the heat flow through the wall

Q = The heat flowing through the unit cell wall or slab

r = Variable radius of the equivalent cylinder model of the unit cell

R = Variable radius of the perforated cylinder

t = Time

T = Temperature

T_o, of fluid

T_b, of the unit cell at radius "b"

T_w, of the unit cell at radius "a" (wall temperature)

T_l, of the slab at length "l"

T(b), a function of "r" evaluated at radius "b"

u = Overall heat transfer coefficient for the unit cell based on heat transfer from radius "b" through the wall to the fluid

u = Radial displacement

U_v = Volumetric heat dissipation coefficient

v = Tangential displacement

x = Variable length of slab

α = Coefficient of expansion

α = Tangential displacement angle

$\beta = \frac{-\alpha E}{1-\mu}$

$\gamma_{r\theta}$ = Shearing strain

ϵ = Strain

ϵ_r, radial strain

ϵ_θ, tangential strain

ϵ_z, axial strain

η = Viscosity of solid material

θ = Denotes tangential conditions

λ_n = Root of $\lambda_n \tan \lambda_n = \frac{hl}{k_0}$ $(n = 0, 1, 2 \ldots\ldots etc)$

μ = Poisson's ratio

$\xi = \left(\frac{\frac{q_{v,n+1}}{k_{n+1}} - \frac{q_{v,n}}{k_n}}{\Delta t} \right)$

π = 3.1416

ρ = Density

σ = Stress

σ_r, radial of unit cell

σ_R, radial of cylinder

σ_θ, tangential

σ_z, axial

τ = Relaxation time, $\tau = \frac{\eta}{G}$

τ_{xy} = Shear stress

ϕ = Stress function